Journal of Medicinal Chemistry

2H-1,2,3-Triazole-Based Dipeptidyl Nitriles: Potent, Selective, and Trypanocidal Rhodesain Inhibitors by Structure-Based Design

Maude Giroud, Bernd Kuhn, Sarah Saint-Auret, Christoph Kuratli, Rainer E Martin, Franz Schuler, François Diederich, Marcel Kaiser, Reto Brun, Tanja Schirmeister, and Wolfgang Haap

J. Med. Chem., **Just Accepted Manuscript** • DOI: 10.1021/acs.jmedchem.7b01870 • Publication Date (Web): 29 Mar 2018

2*H*-1,2,3-Triazole-Based Dipeptidyl Nitriles: Potent, Selective, and Trypanocidal Rhodesain Inhibitors by Structure-Based Design

Maude Giroud, [†] *Bernd Kuhn,* [‡] *Sarah Saint-Auret,* [‡] *Christoph Kuratli,* [‡] *Rainer E. Martin,* [‡] *Franz Schuler,* [‡] *François Diederich,* [†] *Marcel Kaiser,* [§,¥] *Reto Brun,* [§,¥] *Tanja Schirmeister,* [∥]* *Wolfgang Haap*[‡]*

[†]Laboratorium für Organische Chemie, ETH Zurich, Vladimir-Prelog-Weg 3, 8093 Zurich, Switzerland

[‡]Roche Pharma Research and Early Development (pRED), Roche Innovation Center Basel, F. Hoffmann-La Roche Ltd., Grenzacherstrasse 124, 4070 Basel, Switzerland

[§]Swiss Tropical and Public Health Institute, Socinstrasse 57, 4051 Basel, Switzerland

[¥]University of Basel, Petersplatz 1, 4003 Basel, Switzerland

[//]Institut für Pharmazie und Biochemie, Johannes Gutenberg-Universität Mainz, Staudinger Weg 5, 55128 Mainz, Germany

KEYWORDS
rhodesain – African sleeping sickness – dipeptidyl nitrile – trypanosome – triazole – cysteine protease inhibitor – SBDD.

ABSTRACT: Macrocyclic inhibitors of rhodesain (RD), a parasitic cysteine protease and drug target for the treatment of human African trypanosomiasis, had shown low metabolic stability at the macrocyclic ether bridge. A series of acyclic dipeptidyl nitriles was developed using structure-based design (PDB ID: 6EX8). The selectivity against the closely related cysteine protease human cathepsin L (hCatL) was substantially improved, up to 507-fold. In the S2 pocket, 3,4-dichlorophenylalanine residues provided high trypanocidal activities. In the S3 pocket, aromatic residues provided enhanced selectivity against hCatL. RD inhibition (K_i values) and *in vitro* cell-growth of *Trypanosoma brucei rhodesiense* (IC_{50} values) were measured in the nanomolar range. Triazole-based ligands, obtained by a safe, gram-scale flow production of ethyl 1*H*-1,2,3-triazole-4-carboxylate, showed excellent metabolic stability in human liver microsomes and *in vivo* half-lives of up to 1.53 h in mice. When orally administered to infected mice, parasitaemia was reduced but without complete removal of the parasites.

INTRODUCTION

Human African trypanosomiasis (HAT, or African sleeping sickness) is a protozoan infection caused by two subspecies of *Trypanosoma brucei* (*T. b.*): *T. b. gambiense*, responsible for the chronic form of HAT, and *T. b. rhodesiense*, responsible for the more acute form of the disease.[1] HAT consists of two clinical stages, the haemolymphatic stage, which, if left untreated, progresses into stage 2, the neurological stage, when the parasites enter the brain.[2,3] To date, only four therapies exist against HAT which are unsatisfactory because of their costs, toxicity, poor bioavailability, long treatment, and lack of efficacy.[1] Pentamidine and suramin are used against stage 1 HAT, whereas eflornithine, melarsoprol, and, since 2009, the combination therapy

nifurtimox-eflornithine (NECT) are applied to target stage 2.[4] Melarsoprol, an organoarsenic compound, remains the only effective treatment against stage 2 *T. b. rhodesiense* HAT.[1] Because the current treatments present non-neglectable toxicity, there is a need to develop new therapies against this disease, and the Drugs for Neglected Diseases *initiative* (DND*i*) has set up a target product profile with requirements that need to be met for the development of new compounds.[5] Two compounds are currently in clinical trials: fexinidazole,[6] and oxaborole.[7] A third compound, pafuramidine,[8,9] failed in clinical trial. Because of the potential resistance of the parasite towards these new compounds and uncertain outcome of the clinical trials, more research in this field is needed.[10–14]

In this context, we were interested in targeting rhodesain (RD), a trypanosomal cysteine protease implicated in vital functions of the parasite.[15] RD is a human cathepsin L (hCatL)-like cysteine protease produced by *T. b. rhodesiense* and involved in the parasite's iron homeostasis.[16–18] It was also shown that RD is involved in parasite invasivity, allowing it to cross the blood-brain barrier (BBB) of the human host,[19] validating RD as a drug target against HAT.[20] Several classes of inhibitors have been developed against this enzyme,[20] which bind to the protease in either a covalent or a non-covalent manner.

Dipeptidyl nitrile ligands have been described to inhibit a variety of cysteine proteases in a reversible-covalent manner, such as the human cathepsins B,[21,22] C,[23] K,[24] L (e.g. **1**),[25] S,[26] and the parasitic cysteine proteases cruzain (e.g. **1**)[27] or falcipain-2 (Figure 1).[28] Recently, dipeptidyl nitrile **2** was reported to potently inhibit the target enzyme RD (K_i (RD) = 9.2 nM), with significant selectivity against hCatL (SI = 102), however with modest *in vitro* antitrypanosomal activity (8 μM).[29] The electrophilic nitrile functions as head group for nucleophilic attack by the

catalytic cysteine, forming a reversible-covalent thioimidate bond with the protein (schematically shown for **2** in Figure 1).[30]

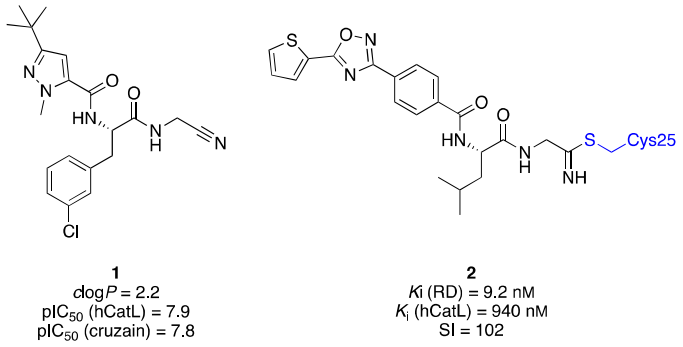

Figure 1. Known dipeptidyl nitriles inhibiting the cysteine proteases hCatL and cruzain (**1**), and RD (**2**). The thioimidate bond formed upon nucleophilic attack by Cys25 of RD is exemplified for **2**.

We recently discovered macrocyclic dipeptidyl nitriles, such as **3**, as potent, trypanocidal RD inhibitors (Figure 2).[31] This ligand class is highly potent on both RD (inhibitory constants K_i down to sub-nanomolar activities) and *T. b. rhodesiense* (half-maximal inhibitory concentration IC_{50} in the subnanomolar range). It did however not prevent complete recovery of the trypanosomes *in vivo*, notably because of the metabolic instability of the ligands, which was attributed to the extended carbon chain of the macrocycle.[31] We therefore aimed at simplifying this scaffold, removing the readily metabolized ether bridge of the macrocycle to increase the *in vivo* exposure and at the same time greatly simplifying the synthetic route. X-ray crystal structures of RD in complex with several macrocycles (PDB IDs:[31] 6EX8, 6EXO, and 6EXQ) enabled the use of structure-based drug design in this quest for new RD inhibitors.

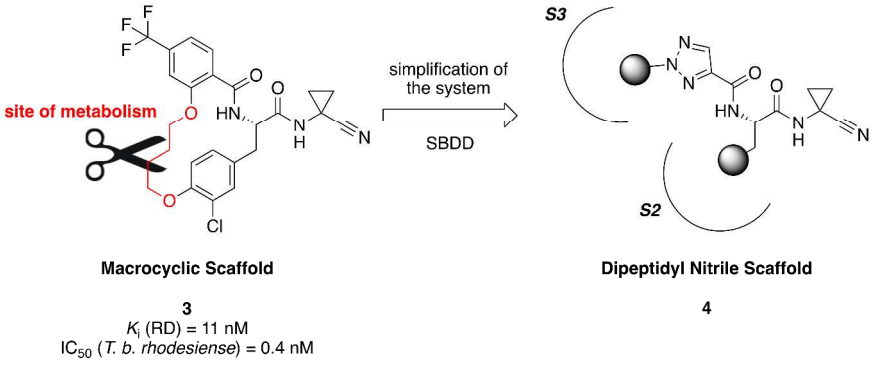

Figure 2. Simplification of the macrocyclic scaffold, as in **3**, towards dipeptidyl nitriles **4**.

Herein, we report the structure-guided design, synthesis, and biological evaluation of 2*H*-1,2,3-triazole-based dipeptidyl nitriles **4** as potent RD inhibitors (Figure 2). Extensive modifications of the substituents addressing the S3 pocket (**5a**–**r**), the S2 pocket (**6a**–**j**, **7a**–**c**), or both (**8a**–**d**) were performed. This required the development of an efficient flow synthesis of a 1,2,3-triazole building block, allowing for gram-scale preparation within short reaction times. The selectivity of the RD inhibitors against the structurally related enzyme hCatL was assessed and the trypanocidal activities determined *in vitro* using a panel of parasites. Selected inhibitors were further evaluated in dose-response recovery assays, their absorption, distribution, metabolism, excretion, and toxicity (ADMET) properties measured, and mouse pharmacokinetics (PK) studies performed. The P-glycoprotein (P-gp) efflux ratio (ER),[32] a crucial parameter for targeting stage 2 HAT, was determined together with the *in vivo* evaluation of the most promising compounds in infected female mice.

RESULTS AND DISCUSSION

Ligand Design. Based on our published crystal structure of macrocycle **3** in complex with RD (PDB ID:[31] 6EX8, 1.6 Å resolution), we removed the –O(CH_2)$_4$O– linker of **3**, which was

previously identified as a site of metabolism.[31] This modification resulted in a typical dipeptidyl nitrile scaffold **4**, exemplified with **5a** (Figure 3). The design of new substituents on scaffold **4** occupying the S2 and S3 pockets of RD was performed with MOLOC using the MAB force field.[33] During the modeling, we kept the protein fixed but allowed for limited flexibility of selected solvent-exposed side chains such as Phe61 in the S3 pocket. The crystal structure of macrocycle **3** in complex with RD revealed a non-covalent binding mode, due to reversible oxidation of the catalytic cysteine to a sulfenic acid (Cys-SOH) under the crystallization conditions.[31] Previously reported crystal structures of dipeptidyl nitriles in complex with the cysteine proteases hCatL (PDB ID:[24] 3HHA, 1.27 Å resolution) and cruzain (PDB ID:[27] 4QH6, 3.13 Å resolution) suggest however, that this type of scaffold binds in a reversible-covalent manner to Cys25, forming a thioimidate bond (Figure S1). Therefore, a covalent bond between Cys25 of RD and the nitrile electrophile with a geometry taken from PDB ID[34] 2XU1 was installed for the modeling studies (Figure 3). The modeled dipeptidyl nitrile scaffold **5a** overlays well with macrocycle **3** in the crystal structure. In the S2 pocket of RD, which preferentially accommodates lipophilic residues,[35] a trifluoromethoxy group was introduced on the phenyl ring in *para* position, aiming at mimicking a part of the macrocyclic linker and stabilizing the phenyl ring against metabolic degradation. The 3-chloro substituent was retained, as it proved to be the best substituent in our macrocyclic series.[31] In our binding mode model, this substituent undergoes favorable dispersive contacts (≤ 4.0 Å) with Leu67 ($d(C_{Leu67}\cdots C–Cl)$ = 3.4 Å, $d(C_{Leu67}\cdots Cl)$ = 3.6 Å), Met68 ($d(C_{Met68}\cdots Cl)$ = 3.5 Å), and Ala208 ($d(C_{Ala208}\cdots Cl)$ = 4.0 Å). The phenyl ring engages in C–H···π interactions with Leu67 on one side and with Ala138 and Leu160 on the other side, at C···C distances between 3.4 to 3.6 Å (Figure S2).

In the macrocyclic series, e.g. in **3**, we had identified an intramolecular hydrogen bond (hereafter referred to as IMHB) between the amide NH of the S3 vector and the adjacent phenol ether O-atom.[36,37] We rationalized this IMHB to be in part responsible for the superior trypanocidal activity of the macrocyclic series in comparison to other ligand classes tested[31] and therefore looked at various heterocycles which could offer a similar hydrogen bonding pattern. In particular, the 1,2,3-triazole motif appeared to be suitable. Our calculations suggest that in the unbound state the IMHB decreases the polar surface area (PSA) of ligand **5a** by ~10 $Å^2$ in comparison to the predicted binding mode (Section S3 in the SI). In addition, the preferred torsion angle τ of N^2-phenyl-1,2,3-triazoles is nearly planar (τ (N–N–C_{phe}–C_{phe}) = 0°–10°) (Figure S3). The agreement with CSD statistics for the torsional preferences of this single bond is support for the binding mode model, but not for the IMHB. The fluoro substituent on the phenyl ring was introduced to provide selectivity against hCatL, as it will closely and unfavorably approach the backbone C=O of Gly61 while the analogous backbone C=O of Ile59 in RD is further away (Figure S4).[34] The fluorophenyl moiety is involved in parallel-shifted π···π stacking with Phe61 at a distance of 3.3–3.5 Å. Furthermore, the triazole N(3) undergoes an orthogonal dipolar interaction with the backbone C=O of Gly66 at the entrance of the pocket at d(N···C=O_{Gly66}) = 3.6 Å, α(N···C=O_{Gly66}) = 62°).

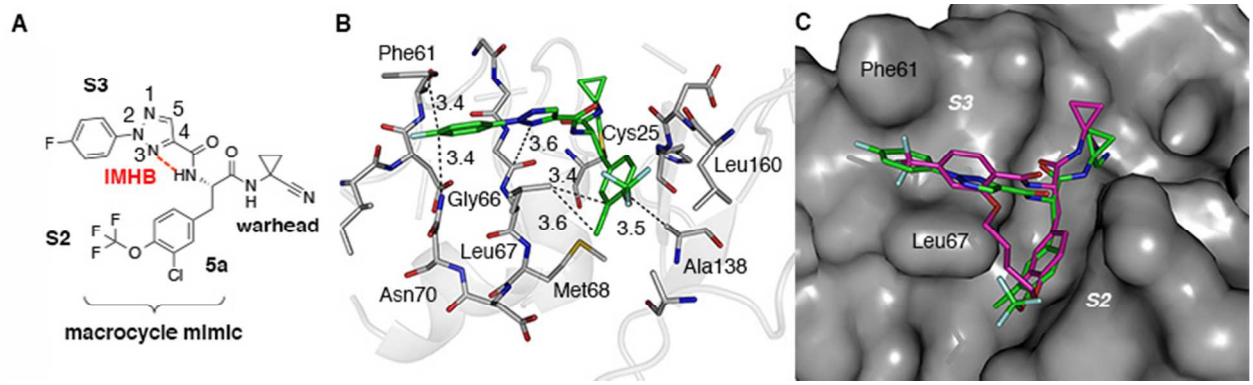

Figure 3. (**A**) Schematic representation of designed dipeptidyl nitrile **5a**; (**B**) predicted binding mode of **5a** in complex with RD (protein coordinates taken from PDB ID:[31] 6EX8, 1.6 Å resolution); (**C**) overlay of the crystal structure of macrocycle **3** in complex with RD (PDB ID:[31] 6EX8, 1.6 Å resolution) with the model of **5a**. Color code: C_3 magenta, C_{5a} green, O red, N blue, F cyan. The protein surface around the active site of RD in the crystal structure is represented in gray.

Synthesis: General Approach. The approach to synthesize the dipeptides **9** consisted in coupling warhead fragment **10** with a carboxylic acid **11**, allowing for rapid derivatization (Scheme 1).

Scheme 1. General Approach for the Preparation of Dipeptides 9.[a]

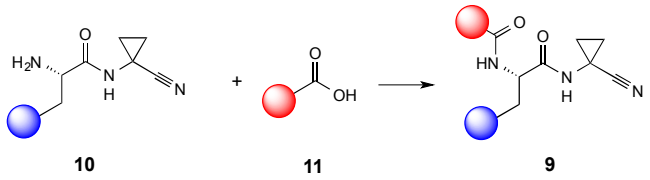

[a] General coupling conditions: HATU, iPr$_2$NEt, DMF. Blue ball: S2 vector; red ball: S3 vector. HATU = 1-[bis(dimethylamino)methylene]-1*H*-1,2,3-triazolo[4,5-b]pyridinium 3-oxide hexafluorophosphate; DMF = *N,N*-dimethylformamide.

Synthesis of 3-Chloro-4-*O*-(trifluoromethyl)-L-tyrosine-Based Dipeptides. The 3-chloro-4-*O*-(trifluoromethyl)-L-tyrosine-based warhead fragment **12** was prepared in a three-steps synthesis (Scheme 2). Commercially available 3-chloro-4-*O*-(trifluoromethyl)-L-tyrosine hydrochloride (**13**) was Boc-protected to give **14** in 65% yield. The nitrile warhead was subsequently introduced *via* amide coupling of aminocyclopropylcarbonitrile hydrochloride and **14** in the presence of HATU and Hünig base to give **15** (65%), which was deprotected using neat formic acid at 23 °C, yielding amine building block **12** quantitatively.

Scheme 2. Preparation of Building Block 12.[a]

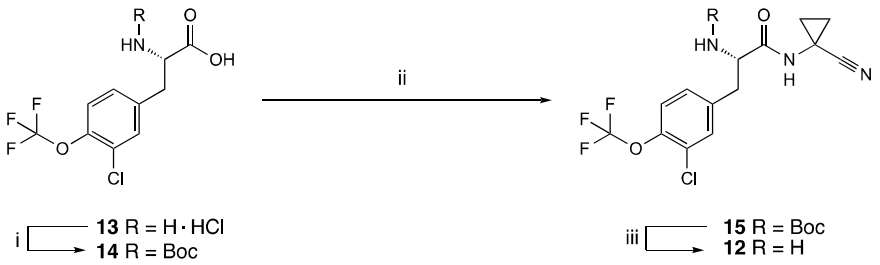

[a]Reagents and conditions: (i) Boc_2O, 1 M NaOH, H_2O/1,4-dioxane 1:1, 16 h at 22 °C, 65%; (ii) 1-aminocyclopropanecarbonitrile hydrochloride, HATU, iPr_2NEt, DMF, 2 h at 22 °C, 65%; (iii) HCOOH, 2.5 h at 22 °C, quant. Boc = *tert*-butoxycarbonyl.

In order to address the S3 pocket of RD with various triazole derivatives, we looked at efficient ways of substituting a 1,2,3-triazole building block at the 2-position. Preparing ethyl 1*H*-1,2,3-triazole-4-carboxylate (**16**) and subsequent derivatization appeared as a promising approach. Based on literature precedence[38–41] and due to safety-related considerations,[42] we opted for a scalable flow preparation of triazole **16**,[43] starting from commercially available trimethylsilyl azide ($TMSN_3$, **17**) and ethyl propiolate (**18**) (Figure 4). Although we initially aimed for running the cycloaddition reaction under classical copper catalysis,[43,44] it became

apparent that the reaction proceeds best in the absence of any copper species, thus avoiding the precipitation of insoluble copper salts that eventually lead to blockage of the system. After rapid optimization, we came up with a plug flow process in which both starting materials trimethylsilyl azide (**17**) and ethyl propiolate (**18**) were injected neat *via* loops (2 mL) every 40 min using acetonitrile as a carrier solvent. Three interlinked perfluoroalkoxy polymer (PTA) reactor coils (each 10 mL) equipped at the exit with a 250-psi back-pressure regulator to maintain system pressure were operated at a temperature of 140 °C. The flow rate of each individual channel was set to 0.5 mL min^{-1}, resulting in a total residence time of 30 min. The product stream was collected, and trituration with diethyl ether provided the triazole **16** as a white solid in 81% isolated yield.

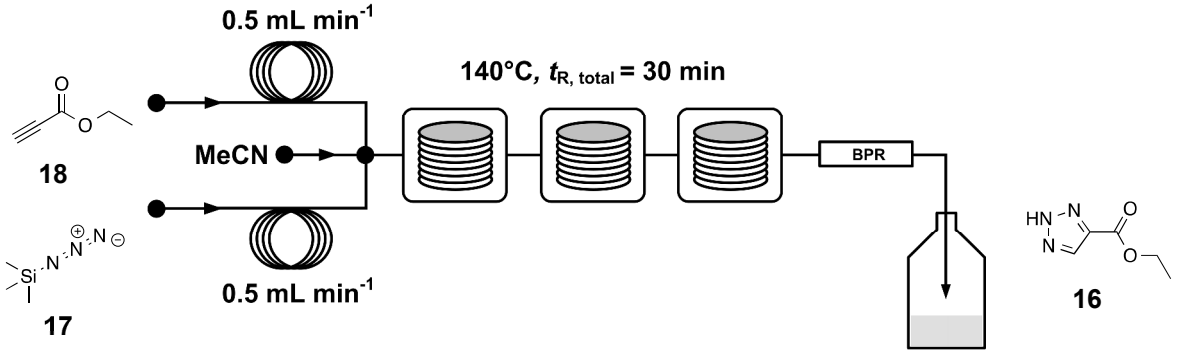

Figure 4. Plug flow process for the production of ethyl 1*H*-1,2,3-triazole-4-carboxylate (**16**).

Procedures for the preparation of N^2-substituted triazoles **19** remain scarce in the literature, and the methods described often lack reliability.[45] We opted for four different approaches: Buchwald-Hartwig-type couplings,[46] Chan-Lam couplings,[47–49] Mitsunobu reaction,[50] and alkylation.[38] *N*-Alkylation or *N*-arylation of **16** with the corresponding aryl or alkyl halides, boronic acids, or alcohols **20c–q** yielded mixtures of N^1/N^2 or N^2/N^3 regioisomers, respectively,

which could easily be separated by flash chromatography (Scheme 3). Buchwald-type aminations led, as reported, exclusively to N^2-substituted triazoles.[46] The N^1-, N^2-, or N^3-substitution pattern of *N*-substituted 1,2,3-triazole-4- or 5-carboxylates was determined based on (i) existing reports,[51–55] (ii) the lower polarity of the N^2-substituted triazoles in comparison to their corresponding regioisomers, and (iii) ^{1}H and ^{13}C NMR, as well ^{15}N-HMBC and NOESY experiments (see Section S4 in the SI for a more detailed analysis). The 2*H*-substituted triazolyl ethyl esters **19c**–**q** were subsequently saponified with LiOH in 2:2:1 H_2O/THF/MeOH, giving carboxylic acids **21c**–**q**. Amide coupling of commercially available **21a**,**b** or **21c**–**q** with amine **12** in the presence of HATU and Hünig base gave dipeptidyl nitriles **5a**–**q**. At last, **5q** was *N*-Boc-deprotected to give compound **5r**.

Scheme 3. Preparation of Dipeptidyl Nitriles 5a–r[a]

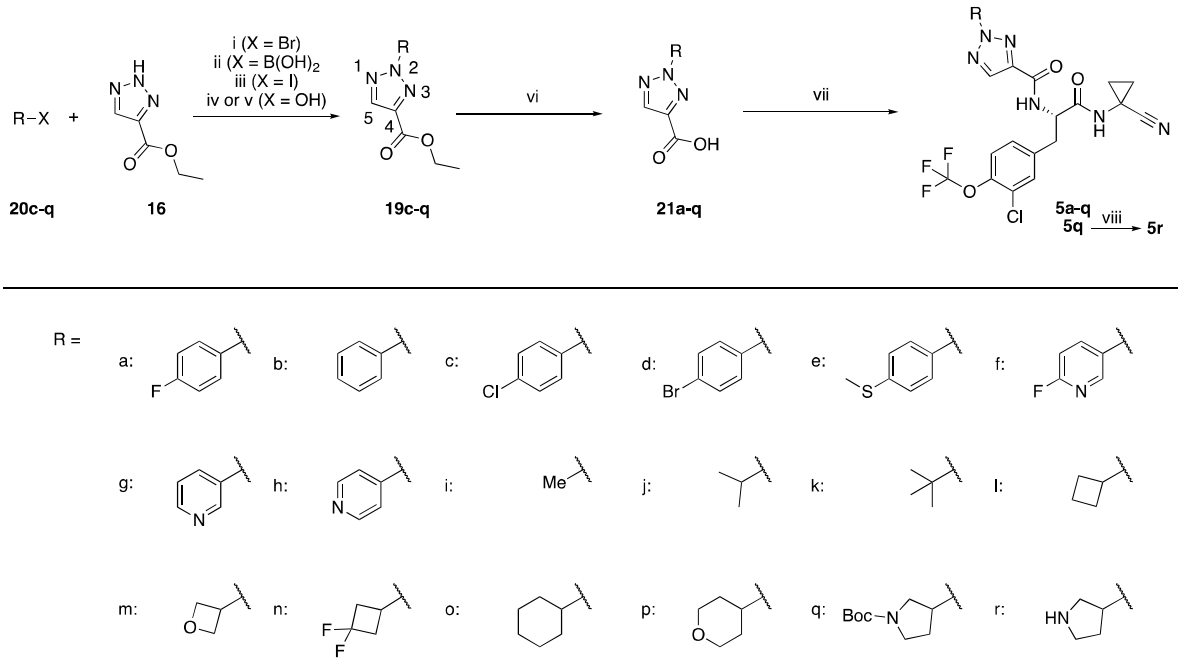

[a] Reagents and conditions: (i) Me_4*t*BuXPhos, [$Pd_2(dba)_3$], K_3PO_4, toluene, 3 h at 90 °C, 4–23%; (ii) $Cu(OAc)_2$, pyridine or KO*t*Bu, DMF or DMA, 48–72 h at 23 °C, 4–12%; (iii) K_2CO_3, MeCN, 18 h at 50 °C, 24%; (iv) 2-(tributylphosphoranylidene)acetonitrile, toluene 1–3 h at 90

°C, 19–38%; (v) *t*BuOH, H_2SO_4, TFA, 5 h at 23 °C, 32%; (vi) LiOH, THF/MeOH/H_2O 2:2:1, 1–2 h at 23 °C, 70–100%; (vii) **12**, HATU, *i*Pr_2NEt, DMF, 1–16 h at 23 °C, 26–74%; (viii) HCOOH, 1 h at 23 °C, 40%. XPhos = 2-dicyclohexylphosphino-2′,4′,6′-triisopropylbiphenyl; dba = (1*E*,4*E*)-1,5-diphenylpenta-1,4-dien-3-one; Ac = acetate; DMA = *N,N*-dimethylacetamide; TFA = trifluoroacetic acid; THF = tetrahydrofuran.

Preparation of 2-(4-Fluorophenyl)-2*H*-1,2,3-Triazole-Based Dipeptides. For this series, the 2-(4-fluorophenyl)-2*H*-1,2,3-triazole motif was kept constant and L-tyrosyl, L-phenylalanyl, and L-leucyl derivatives were introduced. The *N*-Boc protected L-amino acids **22a–j** were coupled with 1-aminocyclopropanecarbonitrile hydrochloride in the presence of HATU and Hünig base to give **23a–j** (Scheme 4). Subsequent deprotection of **23a–j** with neat HCOOH gave the corresponding *N*-(1-cyanocyclopropyl)-L-amino acid derivatives **24a–j**, which were coupled with commercially available 2-(4-fluorophenyl)-2*H*-1,2,3-triazole-4-carboxylic acid (**21a**), yielding final compounds **6a–j**.

Scheme 4. Synthesis of Dipeptidyl Nitriles 6a–j[a]

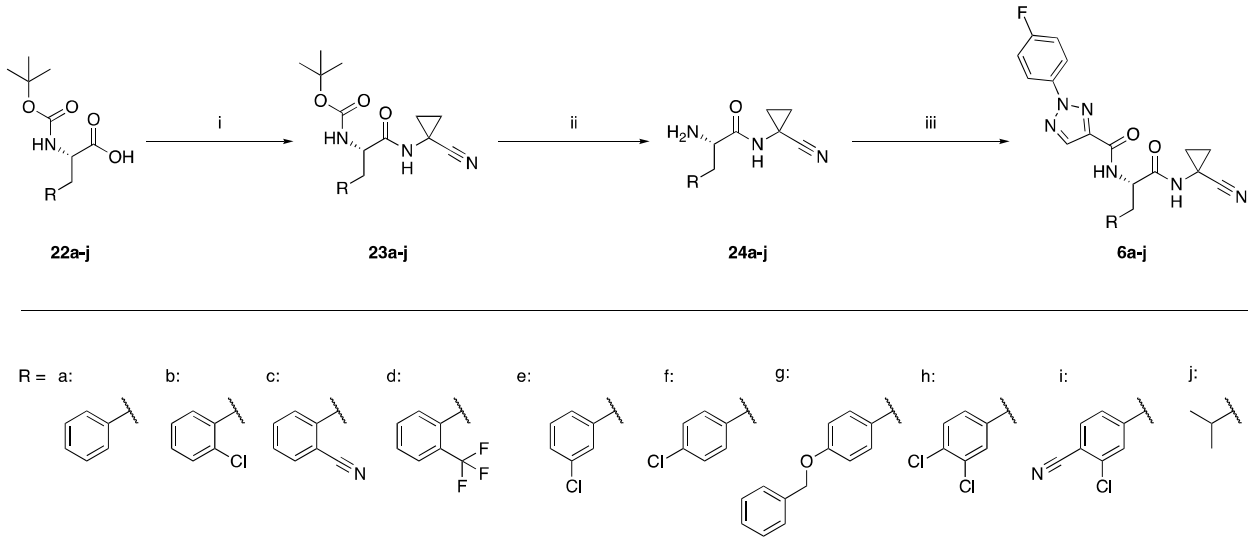

[a]Reagents and conditions: (i) 1-aminocyclopropanecarbonitrile hydrochloride, HATU, *i*Pr_2NEt, DMF, 1–18 h from 0 to 23 °C, 39–98%; (ii) HCOOH, 2.5 h at 23 °C, 83–100%; (iii) 2-(4-fluorophenyl)-2*H*-1,2,3-triazole-4-carboxylic acid, HATU, *i*Pr_2NEt, DMF, 2 h at 0 °C, 25–94%.

O-Alkylated L-tyrosine derivatives **7a**–**c** were prepared in five steps, following an approach similar to the one previously reported (Scheme 5).[31] 3-Chloro-L-tyrosine derivative **25** was treated with Cs_2CO_3 and the corresponding alkyl bromides, to give bis-alkylation products **26a**–**c** in 54–70% yields. Saponification using LiOH afforded carboxylic acids **27a**–**c** in 80% to quantitative yield. Amide coupling with the nitrile head group led to N^{α}-protected-*O*-alkylated L-tyrosine derivatives **28a**–**c** in 44–86% yields. Deprotection with formic acid gave amines **29a**–**c** in 24–52% yields, which were subsequently coupled with 2-(4-fluorophenyl)-2*H*-1,2,3-triazole-4-carboxylic acid (**21a**) to yield dipeptidyl nitriles **7a**–**c** in 24–37% yield.

Scheme 5. Synthesis of Dipeptidyl Nitriles 7a–c[a]

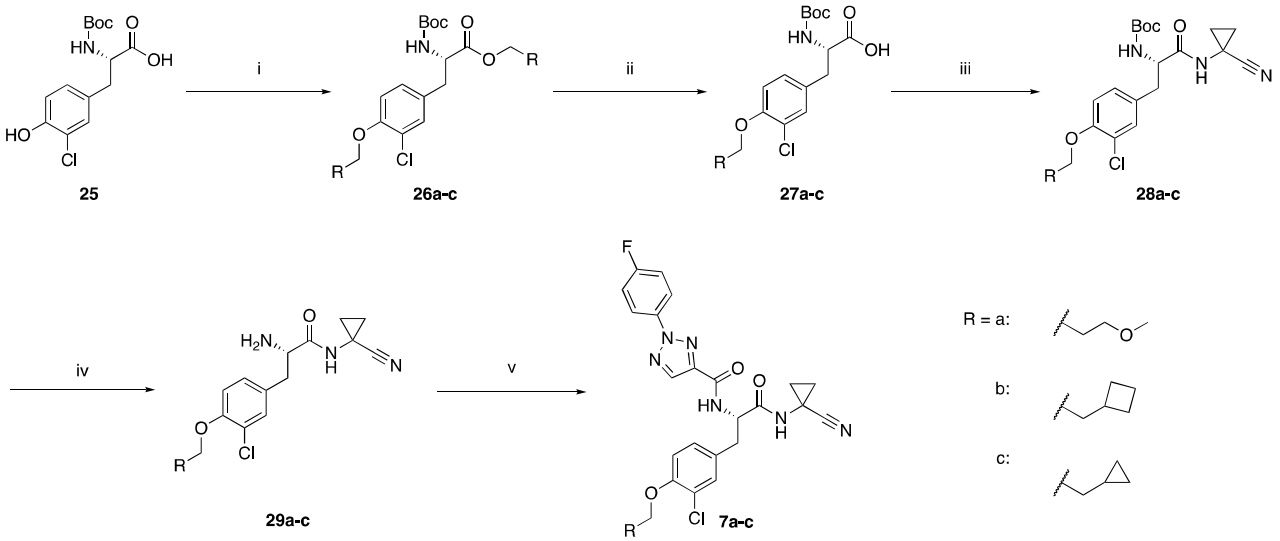

[a]Reagents and conditions: (i) a. Cs_2CO_3, 5 min at 22 °C, b. RCH_2Br, 3–16 h at 22 °C, 54–70%; (ii) LiOH, MeOH/THF/H_2O 2:2:1, 1 h at 22 °C, 80–100%; (iii) 1-aminocyclopropanecarbonitrile hydrochloride, HATU, *i*Pr_2NEt, DMF, 2 h at 0 °C, 44–86%; (iii) HCOOH, 2–4 h at 22 °C, 24–52%; (iv) 2-(4-fluorophenyl)-2*H*-1,2,3-triazole-4-carboxylic acid, HATU, *i*Pr_2NEt, DMF, 2 h at 0 °C, 24–37%.

Preparation of 3,4-Dichloro-L-phenylalanine-based Dipeptides. Amide coupling between carboxylic acids **21l–n**,**p** and L-phenylalanine derivative **24h** provided **8a–d** in 32–56% yield (Scheme 6).

Scheme 6. Synthesis of Dipeptidyl Nitriles 8a–d[a]

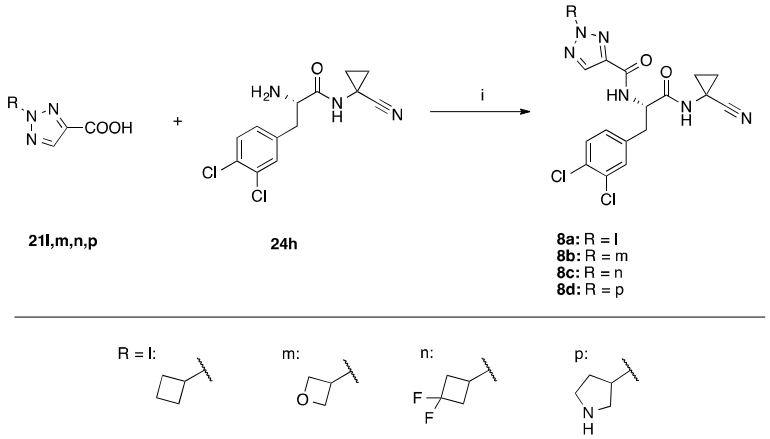

[a]Reagents and conditions: (i) HATU, *i*Pr$_2$NEt, DMF, 2 h at 22 °C, 32–56%.

Biological and Physicochemical Studies. The binding affinities of all ligands reported herein were tested against the cysteine proteases RD and hCatL in a fluorimetric assay (assay buffer for RD: 50 mM sodium acetate pH 5.5, 5 mM EDTA, 200 mM NaCl, and 0.005% Brij35 at 25 °C; assay buffer for hCatL: 50 mM Tris pH 6.5, 5 mM EDTA, 200 mM NaCl, and 0.005% Brij35 at 25 °C), as previously reported.[35,56–58] A selectivity index (SI), defined as SI = K_i (hCatL)/K_i (RD), was determined. In addition, cell-growth inhibition of *T. b. rhodesiense* (IC_{50} (*T. b. rhod.*)) and the cytotoxicity in L-6 rat myoblast cells (IC_{50} (L-6)) were determined in the Alamar Blue® growth inhibition assays.[59] The lipophilicity (log$D_{7.4}$) was determined in a CAMDIS© assay[60] and the solubility in a lyophilization assay (LYSA).[61] The predicted lipophilicity (*c*log$D_{7.4}$) was

calculated with a Roche in-house developed machine-learning tool based on a tree-based ensemble method.

SAR Exploration of 2-Substituted Triazole-based Dipeptidyl Nitriles. Modifying the 2-substituents on the 1,2,3-triazole ring led to potent ligands **5a**–**p**,**r** of RD (K_i = 2.9–93 nM), which efficiently inhibited the cell-growth of *T. b. rhodesiense* (IC_{50} (*T. b. rhodesiense*) = 0.2–67 nM), without being significantly cytotoxic (IC_{50} (L-6) = 7 to > 100 μM) (Table 1, Table S7, and Figure S5 in the SI). Selectivity against hCatL could be obtained by introducing phenyl residues at the 2-position of the triazole ring as in **5a**–**h** (SI = 10–59). Introducing smaller, aliphatic substituents as in **5i**–**p**,**r** led to a decrease or complete loss of selectivity against hCatL. In the *para*-substituted phenyl series **5a**,**c**–**e**, the binding affinities in RD decreased consistently upon increase of the size of the *para*-substituent (H<F<Cl<Br) of the phenyl ring. The same trend was reflected in the binding affinities of hCatL and the cell growth inhibition of *T. b. rhodesiense*. In our binding site models, the *para*-substituent is in close contact with the backbone C=O of Ile59(RD)/Gly61(hCatL) (e.g. for **5a** in RD: $d(C{=}O_{Ile59}\cdots F{-}C)$ = 3.6 Å, $\alpha(C{=}O_{Ile59}\cdots F)$ = 131°). SAR and models suggest that there could be electrostatic repulsion for the fluorine substituent with the backbone carbonyl oxygen and potential steric clashes with the larger para substituents (Figure S4).[56,57] Clearly, the halide SAR does not support any involvement of halogen-bonding interactions. In the pyridyl series **5f–h**, the selectivity against hCatL was reduced (SI = 5–10) in comparison to the phenyl series **5a–e** (SI = 28–59) (Table 1). These compounds **5f–h** were however more potent in the cell-based assay, with 4-pyridine derivative **5h** inhibiting *in vitro* cell growth of *T. b. rhodesiense* in the subnanomolar range (IC_{50} = 0.6 nM). Introduction of aliphatic and heteroalicyclic substituents in **5i–5p,r** on the triazole ring resulted in improved solubility

compared to phenyl derivatives **5a–e**. However, any selectivity against hCatL was lost (Figure S5). Pyrrolidine ligand **5r** was very potent in the *in vitro* cell-growth inhibition assay (IC_{50} (*T. b. rhodesiense*) = 0.2 nM), well soluble (253 µg mL^{-1}), and possessed the highest lipophilic efficiency (LipE = 5.7) of the whole series.

Table 1. Predicted and Experimental Lipophilicity (*c*)log$D_{7.4}$, LYSA Solubility, Inhibition of RD and hCatL, Selectivity Indices (SI), Lipophilic Efficiency (LipE) for RD, Growth Inhibition of *T. brucei rhodesiense*, and Cytotoxicity on L-6 cells of Inhibitors 5a–p,r.

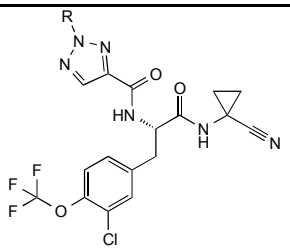

Cpd	R =	*c*log$D_{7.4}$[a]	log$D_{7.4}$[b]	LYSA[c] [µg/mL]	K_i[d] (RD) [nM]	K_i[d] (hCatL) [nM]	SI[e]	LipE[f] (RD)	IC_{50}[g] (*T. b. rhod.)* [nM] (SI[h])	IC_{50}[i] (L-6) [µM]
5a	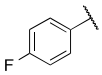	3.7	n.d.	<0.3	7.4	266	36	4.4	9 (2089)	18.8
5b		3.6	n.d.	<0.3	2.9	81.7	28	4.9	5 (3580)	17.9
5c	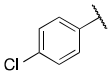	3.7	n.d.	<0.3	10	467	47	4.3	22 (377)	8.3
5d	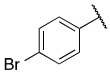	3.8	n.d.	<0.3	25	1076	43	3.8	28 (271)	7.6
5e	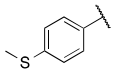	3.8	n.d.	<0.3	19	1116	59	3.9	67 (n.a.[i])	>10

5f	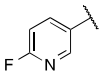	3.8	n.d.	0.5	14	143	10	4.0	6 (1167)	7
5g		3.7	3.70	4.2	36	353	10	3.7	1 (n.a.)	>10
5h		3.7	3.69	5.2	16	82	5	4.1	0.6 (n.a.)	>10
5i		3.1	3.09	53	23	15	0.7	4.5	40 (n.a.)	>10
5j		4.5	4.61	4	18	4	0.2	3.2	4 (n.a.)	>10
5k		4.6	4.87	0.9	31	8	0.3	2.9	4 (1900)	7.6
5l		3.9	3.88	11	11	11	1	4.1	1 (48000)	48
5m		2.6	2.58	4	31	25	0.8	4.9	3 (32000)	96
5n		3.7	3.89	2.2	41	76	1.5	3.7	9 (5556)	50
5o		3.8	n.d.	0.3	12	82	6.8	4.1	6 (5167)	31
5p		3.4	3.33	90	18	112	6.2	4.3	13 (n.a.)	>100
5r		1.3	1.33	253	93	14	0.2	5.7	0.2 (280000)	56

[a] *c*log$D_{7.4}$ calculated with an in-house developed machine-learning tool based on a tree-based ensemble method; [b] log$D_{7.4}$ = intrinsic distribution coefficient between octanol and aqueous buffer (pH 7.4), measured in a CAMDIS© assay; [c] Solubility determined by lyophilization solubility assays (LYSA) at pH 6.5; [d] Average of two measurements, each performed in duplicate. Standard deviations < 10%; [e] SI = selectivity index = K_i (hCatL)/K_i (RD); [f] LipE = pK_i – *c*log$D_{7.4}$; [g] Average of at least 2 measurements, standard deviations < 10%. *T. b. rhodesiense* strain STIB 900, bloodstream form (trypomastigotes); [h] SI = selectivity index relative to the L-6 cells; [i] Average of at least 2 measurements, standard deviations < 10%. Rat skeletal myoblast cell L-6 strain; [j] n.a. = not applicable.

SAR Exploration of the Vector Addressing the S2 Pocket of RD. This series of compounds **6a–j** and **7a–c** led to larger variations in the enzymatic and parasitic activities than those seen in the S3 pocket SAR (Table 2, for all ligands, see Table S8 in the SI). On the enzymatic level, binding affinities ranged from K_i (RD) = 7.4 to 597 nM, with selectivity indices ranging from 18 up to 507. Removing the 3,4-substituents on the phenyl ring of dipeptidyl nitrile **5a** as in **6a** led to a 2.3-fold loss of affinity in RD, 2.4-fold loss in hCatL affinity, and a 57-fold loss in cell growth inhibition, suggesting that the 3,4-substitution pattern of the phenyl ring is critical to achieve reasonable trypanocidal activity. This series **6a–j**, **7a–c** however possesses relatively high log$D_{7.4}$ values, and relatively low solubility, except for L-leucyl ligand **6j**.

2-Substituted L-phenylalanine derivatives **6b–d** led to a decrease in binding affinity in RD and even more pronounced in hCatL in comparison to the unsubstituted derivative **6a** (Table S8). This loss in affinity was also reflected in the *in vitro* cell-growth inhibition, suggesting that 2-substitution of the ring is not ideal for enzymatic or trypanocidal activity. According to molecular modeling, the pocket is narrow in this part of the binding site, potentially leading to repulsive contacts for non-hydrogen substituents (Figure S6 in the SI). 4-Substituted L-phenylalanine derivatives **6f** and **6g** exhibited excellent selectivity over hCatL (SI = 507 for **6f**, SI = 87 for **6g**) and good cell-growth inhibition (**6f**: IC_{50} (*T. b. rhodesiense*) = 6 nM, **6g**: IC_{50} (*T. b. rhodesiense*) = 19 nM) (see Section S5.2 in the SI for a more detailed analysis of the high selectivity of **6f**). 3-Chloro-4-substituted L-phenylalanine or L-tyrosine derivatives **6h–j**, **7a–b** were potent rhodesain inhibitors (K_i (RD) = 2–16 nM). In terms of potency (K_i (RD) = 2 nM, LipE = 5.1), selectivity against hCatL (SI = 66), and cell-growth inhibition (IC_{50} (*T. b. rhodesiense*) = 7 nM), the 3,4-dichlorophenyl derivative **6h** was the best inhibitor of the whole series. On the other hand, L-tyrosine derivatives **7a–c**, although efficient inhibitors of RD (K_i

(RD) = 9–16 nM) and moderate inhibitors of hCatL (K_i (hCatL) = 181–314 nM), were less potent in the *in vitro* cell-based assay (IC_{50} (*T. b. rhodesiense*) = 27–190 nM) compared to the rest of this series. The L-leucyl derivative **6j** did not inhibit RD (K_i (RD) = 23 nM, LipE = 4.3) or the parasitic cell growth (IC_{50} (*T. b. rhodesiense*) = 2.2 μM) as efficiently as the L-tyrosine or L-phenylalanine derivatives, although it was superior in terms of lipophilicity (log$D_{7.4}$ = 3.3) and solubility (LYSA = 42 μg mL^{-1}).

In summary, **6f**, **6h**, and **6i** were the most promising compounds of this SAR. In comparison to macrocycle **3**, they were not only more active on RD, but also more selective against hCatL. In addition, they exhibited high trypanocidal activity (IC_{50} (*T. b. rhodesiense*) < 10 nM).

Table 2. Predicted and Experimental Lipophilicity (*c*)log$D_{7.4}$, Inhibition of RD and hCatL, Selectivity Indices (SI), Lipophilic Efficiency (LipE) for RD, Growth Inhibition of *T. brucei rhodesiense*, and Cytotoxicity on L-6 cells of Selected Inhibitors. LYSA Solubility of Inhibitors Reported in this Table Is < 0.3 μg mL^{-1}.

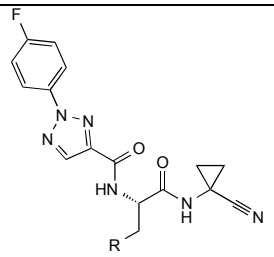

Cpd	R =	*c*log$D_{7.4}$[a]	log$D_{7.4}$[b]	K_i[c] (RD) [nM]	K_i[c] (hCatL) [nM]	SI[d]	LipE[e] (RD)	IC_{50}[f] (*T. b. rhod.)* [nM] (SI[g])	IC_{50}[h] (L-6) [μM]
5a	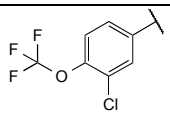	3.7	n.d.	7.4	266	36	4.4	9 (2089)	18.8

6f	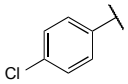	3.7	3.97	3	1522	507	4.8	6 (n.a.[i])	>10
6g	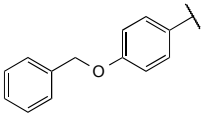	3.6	n.d.	17	1473	87	4.2	19 (n.a.)	>10
6h	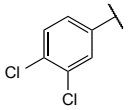	3.6	n.d.	2	131	66	5.1	7 (1386)	9.7
6i	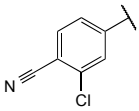	3.5	3.63	7	253	36	4.6	6 (n.a.)	>10
7b	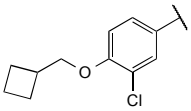	3.6	n.d.	16	314	20	4.2	27 (281)	7.6

[a] *c*log$D_{7.4}$ calculated with an in-house developed machine-learning tool based on a tree-based ensemble method; [b] log$D_{7.4}$ = intrinsic distribution coefficient between octanol and aqueous buffer (pH 7.4), measured in a CAMDIS© assay; [c] Average of two measurements, each performed in duplicate. Standard deviations < 10%; [d] SI = selectivity index = K_i (hCatL)/K_i (RD); [e] LipE = pK_i – *c*log$D_{7.4}$; [f] Average of at least 2 measurements, standard deviations < 10%. *T. b. rhodesiense* strain STIB 900, bloodstream form (trypomastigotes); [g] SI = selectivity index relative to the L-6 cells; [h] Average of at least 2 measurements, standard deviations < 10%. Rat skeletal myoblast cell L-6 strain; [i] n.a. = not applicable.

SAR Exploration of 3,4-Dichloro-L-phenylalanine Derivatives. The 3,4-dichloro-L-phenylalanine derivative **6h** (K_i (RD) = 2 nM, IC_{50} (*T. b. rhodesiense*) = 7 nM) was identified from the S2 pocket SAR as a promising candidate for further optimization. In addition, the 3,4-dichloro-L-phenylalanine possesses the advantage of being a much cheaper building block than the corresponding 3-chloro-4-trifluoromethoxy moiety. We therefore varied the S3 substituents on the 1,2,3-triazole ring. In this subseries, we confirmed that introducing saturated substituents in the S3 pocket decreases the selectivity over hCatL (Table 3). With the exception of **8d** (K_i (RD) = 4 nM, LipE = 5.7), the dipeptidyl nitriles featuring a cyclobutyl (**8a**, K_i (RD) = 71 nM, LipE = 3.5), oxetanyl (**8b**, K_i (RD) = 33 nM, LipE = 5.4), or difluorocyclobutyl (**8c**, K_i (RD) = 18

nM, LipE = 4.3) moiety on the triazole were slightly less active on RD than the corresponding inhibitors possessing a 4-fluorophenyl ring (**6h**, K_i (RD) = 2 nM, LipE = 5.1) in the S3 pocket. However **8a–c** were highly trypanocidal, with IC_{50} values < 10 nM, suggesting that the 3,4-dichloro-L-phenylalanine motif is particularly good for *in vitro* cell-growth inhibition. With *c*log$D_{7.4}$ = 2.1–3.6, they are also less lipophilic than the corresponding 3-chloro-4-*O*-trifluoromethoxy-L-phenylalanine inhibitors **6l–m,p** (*c*log$D_{7.4}$ = 2.6–3.9).

Table 3. Predicted *c*log$D_{7.4}$, Inhibition of RD and hCatL, Selectivity Index (SI), Lipophilic Efficiency (LipE) for RD, Growth Inhibition of *T. b. rhodesiense*, and Cytotoxicity on L-6 Cells of Inhibitors 8a–d.

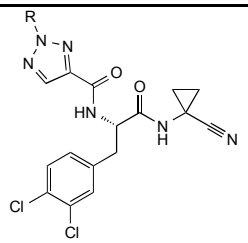

Cmpd	R =	*c*log$D_{7.4}$[a]	K_i[b] (RD) [nM]	K_i[b] (hCatL) [nM]	SI[c]	LipE[d] (RD)	IC_{50}[e] (*T. b. rhod.*) [nM] (SI[f])	IC_{50}[g] (L-6) [μM]
8a		3.6	71	7	0.1	3.5	4 (14550)	58.2
8b		2.1	33	78	2.4	5.4	8 (n.a.[h])	>100
8c		3.4	18	64	3.6	4.3	8 (6844)	54.75
8d		2.7	4	93	23	5.7	23 (n.a.)	>100

[a] *c*log$D_{7.4}$ calculated with an in-house developed machine-learning tool based on a tree-based ensemble method; [b] Average of two measurements, each performed in duplicate. Standard

deviations < 10%; [c] SI = selectivity index = K_i (hCatL)/K_i (RD); [d] LipE = pK_i – *c*log$D_{7.4}$; [e] Average of at least 2 measurements, standard deviations < 10%. *T. b. rhodesiense* strain STIB 900, bloodstream form (trypomastigotes); [f] SI = selectivity index relative to the L-6 cells; [g] Average of at least 2 measurements, standard deviations < 10%. Rat skeletal myoblast cell L-6 strain; [h] n.a. = not applicable.

Reversibility of Drug Effect. In addition to the IC_{50} determination in the standard 72 h assay,[62] the reversibility of drug effect was examined. Pulse incubation of *T. b. rhodesiense* with **5a** and **5b** shows that at least a 24 h drug pressure is required to produce an irreversible effect on parasite survival (Table 4). Melarsoprol, one of the few commercially available drugs against HAT,[63] was used as a standard. Inhibitor **5a** (IC_{50} (48 h) = 0.064 μM) was still inhibiting the cell-growth after 48 h incubation, comparable to melarsoprol (IC_{50} (48 h) = 0.026 μM), and superior to inhibitor **5b** (IC_{50}(48 h) = 0.462 μM).

Table 4. Dose-response Recovery of 5a,b Against *T. brucei rhodesiense*.

	IC_{50} (*T. b. rhodesiense*) [μM][a]				
Cpd	**2 h**	**6 h**	**16 h**	**24 h**	**48 h**
5a	>1	>1	>1	0.45	0.064
5b	>1	>1	>1	0.556	0.462
Melarsoprol	>0.18	0.099	0.086	0.044	0.026

[a] Average of at least 2 measurements, standard deviations < 10%. *T. b. rhodesiense* strain STIB 900, bloodstream form (trypomastigotes)

Drug Metabolism and Pharmacokinetics. Key physicochemical parameters (Table 5), and mouse pharmacokinetics (Table 6) were determined for a set of dipeptidyl nitriles with promising *in vitro* antitrypanosomal activities.

These compounds possess low *in vitro* human and mice microsomal clearances, consistent with good metabolic stability (Table 5). Their octanol-water distribution coefficient (log$D_{7.4}$) was lower than the threshold of 5 set by the DND*i*'s target product profile,[5] however they were

poorly soluble (LYSA < 1 μg/mL), except for **5i** (LYSA = 53 μg/mL). The PAMPA values showed a relatively low permeability, except for **5k** (28.6 nm s^{-1}) and **6h** (10.7 nm s^{-1}). The compounds did not significantly inhibit CYP3A4 or CYP2C9, but were inhibiting CYP2D6 in the low μM range.

According to the target product profile,[5] the PSA should be ≤ 85 $Å^2$ to promote good brain penetration. Polar surface areas were generally calculated using the MOLOC[33] companion program Msrfvl based on a low-energy conformation generated with the MOLOC[33] program Mol3d (Table 5, see Table S1 in the SI for all data). To explore how useful the Mol3d based conformations are for PSA calculations, we investigated the dipeptidyl nitrile **5a** in more detail. Figure 5 shows model conformations representative of the bound and unbound states, respectively. In particular, Figure 5A shows a model of the bound state in RD derived from the predicted binding mode in Figure 3. The PSA is 108.9 $Å^2$, and no intramolecular hydrogen bond is apparent. Figure 5B shows the low energy conformation in the unbound state generated with Mol3d, which is using a molecular mechanics (MM) based representation. Two intramolecular hydrogen bonds are visible and the predicted PSA is 107.3 $Å^2$. We compared this with a more sophisticated approach using a MM conformational search (Maestro version 2016-4, OPLS3 force field, implicit solvent $CHCl_3$) followed by a quantum-mechanical (QM) optimization (Gaussian 09 Rev. D.01, B3LYP/cc-pVDZ, implicit solvent $CHCl_3$) of all conformers below an energy cutoff ΔE_{MM}: 3.0 kcal/mol (RMSD cutoff: 0.5 Å). The resulting conformer with lowest QM energy is depicted in Figure 5C. While the overall conformation is different compared to the pure MM approach (Figure 5B) the same two intramolecular hydrogen bonds are formed. The PSA for the QM calculated conformation is 99.9 $Å^2$, which is roughly 10 $Å^2$ smaller compared to the bound state (Figure 5A). In comparison, a 2D TPSA calculation[64] for this molecule yields

121.9 Å^2, which is strongly overestimating the 3D QM-based value. From this analysis, we conclude that 2D TPSA values are not suitable for this system involving several intramolecular hydrogen bonds. The PSA was reduced by about 10 Å^2 when replacing the 4-trifluoromethoxy group as in **5a** by a 4-chloro-substituent as in **6h**, while other properties were very similar (Table 5), suggesting that the 3,4-dichloro-L-phenylalanine motif could be the most suitable choice for further optimizations.

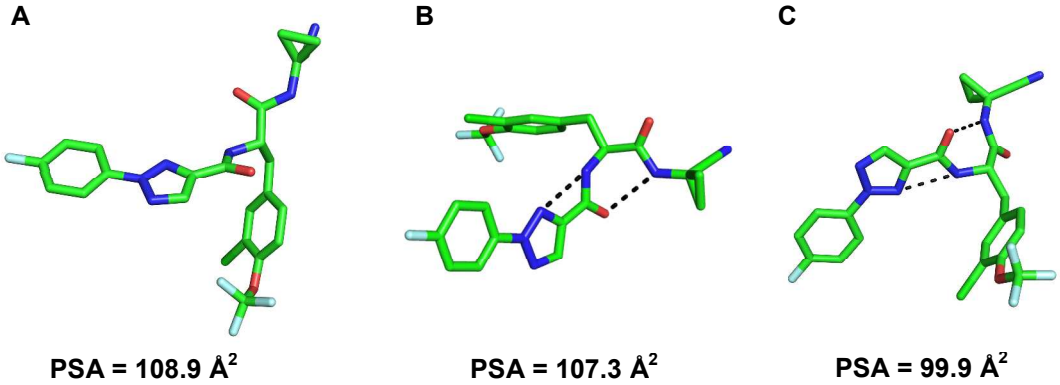

Figure 5. Conformation of dipeptidyl nitrile **5a** in the (**A**) bound conformation (extracted from the predicted binding mode in RD, protein coordinates taken from PDB ID:[3] 6EX8, 1.6 Å resolution); (**B**) low energy conformation in the unbound state generated with Mol3d; (**C**) unbound conformation using a MM conformational search with subsequent QM optimization. Polar surface areas were calculated with the MOLOC companion program Msrfvl. Color code: green $C_{\mathbf{5a},bound}$, cyan $C_{\mathbf{5a},unbound}$, red O, blue N, lime Cl, light blue F. Distances represented by dotted black lines and given in Å.

Table 5. *In Vitro* Data for Selected Compounds.

	5a	**5f**	**5g**	**5i**	**5j**	**5k**	**6h**
IC_{50}[a] (*T. b. rhod.*) [nM]	9	6	1	40	4	4	7
IC_{50}[b] (L-6 cells) [μM]	>10	6.99	>10	>10	>10	7.63	9.67
hCl[c]	<10	<10	<10	<10	11	<10	<10
mCl[c]	<10	<10	11	<10	26	17	<10
$\log D_{7.4}$[d]	n.d.	n.d.	3.70	3.09	4.61	4.87	n.d.
LYSA[e]	<0.3	0.5	4.2	53	4	0.9	<0.3
PAMPA[f]	n.d.	2.91	4.47	1.2	1.38	28.62	10.72
CYP IC_{50} [μM] 3A4/2D6/2C9	>50/3/9	47/1/11	8/2/7	>50/6/>50	n.d.	>50/0.5/5	>50/5/4
PSA[g] [$Å^2$]	107.3	119.1	116.1	109.2	105.2	107.2	98.9
HBD[h]	2	2	2	2	2	2	2
HBA[i]	9	10	10	9	9	9	8

[a] Average of at least 2 measurements, standard deviations < 10%. *T. b. rhodesiense* strain STIB 900, bloodstream form (trypomastigotes); [b] Average of at least 2 measurements, standard deviations < 10%. Rat skeletal myoblast cell L-6 strain; [c] Microsomal intrinsic clearances [$\mu L\ min^{-1}\ mg^{-1}$] in human (h) and mouse (m); [d] $\log D_{7.4}$ = intrinsic distribution coefficient between octanol and aqueous buffer (p*H* 7.4), measured in a CAMDIS© assay; [e] Solubility determined by lyophilisation solubility assays (LYSA) at p*H* 6.5; [f] Membrane permeability [$nm\ s^{-1}$] derived from the PAMPA assay; [g] Polar Surface Area [$Å^2$] calculated using Mol3d/Msrfvl; [h] Number of hydrogen-bond donors; [i] Number of hydrogen-bond acceptors.

The PK profile of these compounds was further characterized in mice, following intravenous administration (Table 6, Section S6 in the SI). Compounds **5a** and **6h** possessed relatively flat curves, and therefore no complete area under the curve could be determined (Section S6 in the SI). For the remaining dipeptidyl nitriles, the half-lifes ($t_{1/2}$) spanned from 0.94–1.53 h, and the clearances (CL) from 10.2–32.9 mL $min^{-1}\ kg^{-1}$. Finally, the unbound fraction of plasma protein binding was between 1.48 % for **5f** to 22.64 % for **5i**. In comparison to our macrocyclic series,[31]

the half-life was slightly reduced. All compounds possess a fraction unbound (%f_u) in the plasma protein binding assay which is in the typical range for good drugs.

Table 6. Mouse Pharmacokinetic Profile of Selected Compounds.

	5a	**5f**	**5g**	**5i**	**5j**	**5k**	**6h**
Route	i.v.	i.v.	i.v.	i.v.	i.v.	i.v.	i.v.
Dose [mg kg^{-1}]	1.2	0.8	1.5	1.5	1.5	1.3	1.3
$t_{1/2}$ [h]	n.d.	1.42	0.94	1.52	1.53	1.30	>6.4
CL [mL min^{-1} kg^{-1}]	n.d.	10.2	22.6	22.8	32.9	17	<4.6
V_{ss} [L kg^{-1}]	n.d.	1.2	0.8	2.7	3.0	1.7	<2.5
AUCpo/D [ng h mL^{-1}]	n.d.	1627	738	730	507	983	>3611
PPB human %f_u[a]	n.d.	1.48	3.95	22.64	8.26	n.d.	n.d.

[a] Plasma protein binding, fraction unbound.

Brain Penetration of Dipeptidyl Nitriles. The ability of a drug to cross the BBB is crucial if intended to treat stage 2 HAT.[65] The P-glycoprotein (P-gp) efflux ratio (ER) (one of the parameters used to evaluate brain penetration) of dipeptidyl nitrile **5a** was determined in LLCPK1 cells stably expressing human MDR1 (Table 7). This ER was improved by a factor 4.3 in human for **5a** (ER = 6 in human) in comparison to macrocycle **3** (ER = 26), and by a factor 2.7 in mice. This improvement is remarkable, especially taking into account the predicted PSA of the respective compounds (PSA = 107.3 Å^2 for **5a**, and PSA = 80.2 Å^2 for **3**).

Table 7. P-Glycoprotein (P-gp) Efflux Ratio (ER) and Estimated PSA of Selected Inhibitors.

	P-gp Human ER[a]	P-gp Mouse ER[b]	PSA [Å^2]
3	26	53	80.2[c]
5a	6	20	107.3[c]

[a] Human efflux ratio (ER) in LLCPK1 cells stably expressing human MDR1; [b] Mouse efflux ratio (ER) in LLCPK1 cells stably expressing mouse Mdr1a; [c] PSA [Å^2] = polar surface area.

Antiparasitic Activity Against Other Parasites and Cytotoxicity. The *in vitro* cell-growth inhibition of dipeptidyl nitriles **5c–p,r**, **6a–j**, **7a–c**, **8a–d** was determined for a panel of protozoan parasites consisting, in addition to *T. b. rhodesiense* (Section S7 in the SI), of *Leishmania donovani*, *T. cruzi*, and *Plasmodium falciparum*, the causative agents of Leishmaniasis,[66] Chagas' disease,[67] and malaria tropica,[68] respectively. The IC_{50} values obtained by using the corresponding typical antiprotozoal drugs are reported as mean of comparison. All compounds presented good to excellent selectivity against the other parasites, suggesting that our inhibitors selectively target RD, despite the structural similarities with the parasitic enzymes cruzain[27] (from *T. cruzi*), falcipain-2[28] (from *P. falciparum*), and *Leishmania* cysteine proteases.[66] In addition, they all possess moderate to low cytotoxicity, as demonstrated by the IC_{50} values against L-6 rat myoblast cells.

***In Vivo* Evaluation of Selected Dipeptidyl Nitriles.** Based on the reported *in vitro* data, we selected inhibitors **5f**, **5h**, **5i**, **5m**, **5r**, **6h**, **8b**, and **8c** for *in vivo* evaluation. The compounds were dissolved in DMSO/H_2O and orally administered in female mice on three consecutive days at a dose of 50 mg/kg/day, beginning 24 h post infection (Table 8, for full data set, see Section S8 in the SI). Despite their *in vitro* potencies, none of the compounds cured any infected mice. 6 out of

8 *in vivo* tested compounds exhibited some activity (**5f**, **5h**, **5i**, **5m**, **6h**, and **8b**) and did cause a reduction in parasitaemia of 45–54 % at 24 h after the final dose. This limited activity may be due to insufficient systemic drug exposure despite the rather high daily doses. Based on their in vitro solubility, permeability and metabolic stability data it can be assumed that the compounds are incompletely absorbed and/or too rapidly eliminated which would result in sub-efficacious exposure over the dosing interval. In order to improve these results, increasing the *in vivo* exposure of the compounds would be required. In particular, replacing one amide bond by an amide isoster, as performed for the development of cruzain inhibitors, would be a next step to be undertaken.[67]

Table 8. *In Vivo* Evaluation of a Set of Dipeptides Orally Administered to Female Mice Infected with *T. b. rhodesiense* (STIB900). Values are means of 2 mice, and 4 mice were included in the untreated control group.

Cpd	Dose [mg kg^{-1}]	Parasites / µL of blood	% of control	% of activity[a]
Ctrl	untreated	224500		
5f	3 x 50	132850	59.2	40.8
5h	3 x 50	127250	56.7	43.3
5i	3 x 50	104000	46.4	53.6
5m	3 x 50	127710	56.9	43.1
5r	3 x 50	223500	99.6	0.4
6h	3 x 50	118330	52.8	47.2
8b	3 x 50	122890	54.7	45.3
8c	3 x 50	189000	84.2	15.8

[a] Activity represents the reduction of parasitaemia compared with untreated controls.

CONCLUSIONS

A series of triazole-based dipeptides as second-generation RD inhibitors was designed, starting from the crystal structure of macrocycle **3** in complex with RD (PDB ID:[31] 6EX8, 1.6 Å resolution). We explored SARs in the S2 and S3 pockets of RD, paying attention to (i) increasing the selectivity against hCatL and (ii) improving the metabolic stability of the compounds. The preparation of these inhibitors required the development of a safe, scalable, gram-scale flow production of ethyl 1*H*-1,2,3-triazole-4-carboxylate (**16**). These triazole-based dipeptides displayed excellent *in vitro* trypanocidal activities against the STIB 900 laboratory strain of *T. b. rhodesiense*, and dipeptidyl nitriles **5h** and **5r** possessed subnanomolar cell-growth inhibition of *T. brucei rhodesiense*. Such activities are superior to clinical candidate fexinidazole (IC_{50} = 1.71–2.93 μM) or currently used drugs eflornithine (IC_{50} = 3.80 μM), nifurtimox (IC_{50} = 1.44 μM), and suramin (IC_{50} = 0.046 μM), and are comparable to melarsoprol (IC_{50} = 0.004–0.009 μM) and pentamidine (IC_{50} = 0.009 μM). In addition, they presented low to moderate cytotoxicity on L-6 cells. Compound **5a** inhibited the cell-growth of *T. b. rhodesiense* after 48 h incubation (IC_{50} (48 h) = 0.064 μM). The pharmacokinetic profile of these compounds was comparable to the macrocyclic series. Remarkably, the P-gp efflux ratio of dipeptidyl nitrile **5a** was improved by a factor 4.3 in human in comparison to macrocycle **3**, and by a factor 2.7 in mice. Upon oral administration, compounds **5f**, **5h**, and **6h** reduced *in vivo* the parasitaemia by 40–47% compared to untreated mice. We believe that the reported inhibitors are a promising source for further derivatization. We will look for other heterocycles addressing the S3 pocket at first. Subsequently, we intend installing amide isosters in order to improve the bioavailability of the compounds. This has proven effective in the development of odanacatib, a cathepsin K inhibitor, or cruzain inhibitors.[67]

EXPERIMENTAL SECTION

Chemical Synthesis. Only the synthesis and characterization of selected final compounds **5f**, **5h**, **7b**, and **8c** are described herein, together with the corresponding general procedures (GP). More information about the general methods and materials, synthesis of all intermediates, and characterization, can be found in Section S9 in the SI. The purity of all compounds reported here was assessed by NMR and LC-MS, and was identified as > 95%. The NMR spectra of all reported final compounds are reported in Section S10 in the SI.

General Procedures (GP). *GP-1: Saponification.* A solution of the ester (1.0 eq) in THF/MeOH/H_2O 2:2:1 (170 mM) was treated with LiOH (2.0 eq), stirred for 1–4 h at 22 °C, and poured onto 0.1 M HCl. The aqueous phase was extracted with CH_2Cl_2. The organic layer was dried over Na_2SO_4, filtered off, and evaporated. MPLC gave the corresponding carboxylic acids, or the crude acid was directly used in the next step

GP-2: Amide coupling. A solution of amine (1 eq), carboxylic acid (1 eq), and HATU (2 eq) in DMF (130 mM) was treated with *i*Pr_2NEt (4 eq), stirred for 3–18 h at 22 °C under Ar, treated with a sat. aq. $NaHCO_3$ solution, and diluted with EtOAc. The organic phase was washed with brine (3x), dried over Na_2SO_4, filtered, and evaporated. The compounds were purified by MPLC or HPLC.

GP-3: N-Boc deprotection. A solution of protected amine (1 eq) in HCOOH (250 mM) was stirred for 1–4 h at 22 °C, diluted with CH_2Cl_2/H_2O 4:1, basified to pH 9, and extracted with CH_2Cl_2 (3x). The combined organic layers were dried over Na_2SO_4, filtered, and evaporated to afford the crude corresponding amines.

*GP-4: Buchwald-Hartwig coupling of triazole **16** and bromophenyl derivatives.* A flame-dried flask was equipped with a magnetic stir bar and charged with [$Pd_2(dba)_3$] (0.01 eq) and

Me_4*t*BuXPhos (0.02 eq). The flask was evacuated and backfilled with Ar (3x). Toluene (435 mM) was added, and the resulting mixture was stirred for 3 min at 120 °C until the color turned from dark-purple to dark-brown. A second, previously dried flask, was equipped with a stir bar, and charged with K_3PO_4 (2 eq) and triazole **16** (1.2 eq). The flask was evacuated and back-filled with Ar (3x). The bromophenyl derivative (1 eq) was then added, as well as the premixed catalyst solution and additional toluene (435 mM). The mixture was heated to 120 °C for 3–5 h, before being cooled down to 25 °C, and diluted with EtOAc. The organic layer was washed with brine, dried over Mg_2SO_4, filtered, and evaporated. The residue was purified by MPLC.

*GP-5: Chan-Lam coupling of triazole **16** and boronic acids.* A solution of triazole **16** (1.0 eq), boronic acid (2 eq), $Cu(OAc)_2$ (2 eq) and pyridine (2 eq) or KO*t*Bu (2 eq) in DMF or DMA (230–250 mM) was stirred for 22–72 h at 25°C, before being filtered through a silica plug. The filtrate was evaporated and the residue purified by MPLC.

GP-6: Mitsunobu reaction. A solution of **16** (1 eq), alcohol (1.5 eq), and 2-(tributylphosphoranylidene)acetonitrile (1 eq) in toluene (140 mM) was stirred for 2 h at 80 °C, and evaporated. A solution of the residue in EtOAc was washed with H_2O (1x), brine (2x), dried over Na_2SO_4, filtered off, and evaporated. The corresponding 1*H*- and 2*H*-subsituted triazoles were purified by MPLC.

GP-7: O-Alkylation of 3-chloro-L-tyrosine derivatives. A solution of 3-chloro-L-tyrosine derivative (1.0 eq) in dry DMF (290 mM) was treated with Cs_2CO_3 (2.1 eq), stirred for 5 min at 22 °C under Ar, treated with allyl bromide or 1-bromobut-2-yne (2.1 eq), and stirred for 4–16 h. The mixture was diluted with EtOAc, washed with brine (3 x), dried over Na_2SO_4, filtered off, and evaporated. The residues were purified by MPLC.

***N*-(1-Cyanocyclopropyl)-3-chloro-4-*O*-(trifluoromethyl)-*N*$^{\alpha}$-[(2-(6-fluoropyridin-3-yl)-2*H*-triazol-4-ylcarbonyl]-L-tyrosinamide (5f).** A solution of **19f** (30 mg, 0.13 mmol) in THF/MeOH/H_2O 2:2:1 (1.25 mL) was treated with LiOH (6 mg, 0.25 mmol) according to GP-1. Acid **21f** (30 mg, 95%) was obtained as a white solid, which was directly used in the next step. A solution of **21f** (60 mg, 0.17 mmol) in DMF (2.5 mL) was treated with **12** (30 mg, 0.14 mmol), HATU (110 mg, 0.29 mmol), and *i*Pr_2NEt (88 μL, 0.50 mmol), according to GP-2. MPLC (SiO_2; heptane/EtOAc, gradient from 100:0 to 50:50 within 30 min) and RP-HPLC (C18 column, 70:30 MeCN/H_2O + 0.05% Et_3N) gave **5f** (22 mg, 28%) as a white solid. R_f = 0.86 (SiO_2; CH_2Cl_2/MeOH 9:1, UV 254 nm). $[\alpha]_D^{20}$ –32.9 (*c* 1.0, MeOH). ^{1}H NMR (600 MHz, $(CD_3)_2SO$): δ = 0.99–1.09 (m, 2 H; H_a–C(2,3) of cyclopropyl), 1.47–1.51 (m, 2 H; H_a–C(2,3) of cyclopropyl), 3.08 (dd, *J* = 13.7, 9.5 Hz, 1 H; H_a–C(β)), 3.15 (dd, *J* = 13.7, 5.5 Hz, 1 H; H_b–C(β)), 4.66 (ddd, *J* = 9.6, 8.3, 5.6 Hz, 1 H; H–C(α)), 7.37 (dd, *J* = 8.5, 2.1 Hz, 1 H; H–C(6)), 7.46 (dq, *J* = 8.4 Hz, ^5J(H,F) = 1.5 Hz, 1 H; H–C(5)), 7.51 (dd, *J* = 8.9 Hz, ^3J(H,F) = 2.9 Hz, 1 H; H–C(5'')), 7.62 (d, *J* = 2.1 Hz, H–C(2)), 8.52 (s, 1 H; H–C(5')), 8.63 (ddd, *J* = 9.4 Hz, ^4J(H,F) = 6.8 Hz, *J* = 2.8 Hz, 1 H; H–C(4'')), 8.95 (br s, 1 H; H–C(2'')), 8.97 (br s, 1 H; HN–C(α)), 9.10 ppm (s, 1 H; NH). ^{13}C NMR (151 MHz, $(CD_3)_2SO$): δ = 15.57 and 15.65 (2 C; C(2,3) of cyclopropyl), 19.73 (C(1) of cyclopropyl), 35.89 (C(β)), 53.56 (C(α)), 110.92 (d, ^2J(C,F) = 39.9 Hz; C(5'')), 120.01 (q, ^1J(C,F) = 258.0 Hz; CF_3), 120.56 (CN), 122.87 (C(5)), 125.50 (C(3)), 129.81 (C(6)), 131.64 (C(2)), 133.23 (d, ^3J(C,F) = 9.0 Hz; C(4'')), 134.10 (d, ^4J(C,F) = 4.6 Hz; C(3'')), 137.09 (C(5')), 138.29 (d, ^3J(C,F) = 16.8 Hz; C(2'')), 139.11 (C(1)), 142.60 (q, ^3J(C,F) = 1.7 Hz; C(4)), 144.14 (C(4')), 158.75 (O=*C*–C(4')), 161.99 (d, ^1J(C,F) = 238.1 Hz; C(6'')), 171.62 ppm (O=*C*–C(α)). ^{19}F{^{1}H} NMR (377 MHz, $(CD_3)_2SO$): δ = –68.71 (F–C(6'')), –57.08 ppm (CF_3). IR (ATR): $\tilde{\nu}$ = 3257 (w), 3047 (w), 2244 (w), 1672

(s), 1649 (s), 1607 (w), 1536 (m), 1498 (s), 1486 (m), 1437 (w), 1418 (w), 1400 (w), 1371 (m), 1320 (w), 1298 (w), 1262 (s), 1245 (s), 1217 (s), 1203 (s), 1157 (s), 1079 (w), 1060 (w), 1039 (w), 1023 (w), 993 (w), 968 (m), 910 (m), 860 (s), 850 (m), 836 (m), 804 (w), 769 (m), 685 (s), 675 (s), 666 (s), 635 cm^{-1} (m). HR-ESI-MS: *m/z* (%): 536.0885 (100, $[M + H]^+$, calcd for $C_{22}H_{15}{}^{35}ClF_4N_7O_3^-$: 536.0867).

3-Chloro-*N*-(1-cyanocyclopropyl)-*N*$^{\alpha}$-[(2-(pyridin-4-yl)-2*H*-1,2,3-triazol-4-ylcarbonyl]-4-*O*-(trifluoromethyl)-L-tyrosinamide (5h). A solution of **12** (55 mg, 0.16 mmol) in DMF (1 mL) was treated with acid **21h** (30 mg, 0.16 mmol), HATU (120 mg, 0.32 mmol), and *i*Pr_2NEt (96 µL, 0.55 mmol) according to GP-2. MPLC (SiO_2; CH_2Cl_2/MeOH, gradient from 100:0 to 90:10 within 30 min) gave **5h** (49 mg, 60%) as a white solid. R_f = 0.81 (SiO_2; CH_2Cl_2/MeOH 9:1, UV 254 nm). m.p. 141–145 °C. $[\alpha]_D^{20}$ –35.5 (*c* 0.1, MeOH). ^{1}H NMR (600 MHz, $(CD_3)_2SO$): δ = 1.00–1.09 (m, 2 H; H_a–C(2,3) of cyclopropyl), 1.47–1.51 (m, 2 H; H_b–C(2,3) of cyclopropyl), 3.09 (dd, *J* = 13.7, 9.5 Hz, 1 H; H_a–C(β)), 3.16 (dd, *J* = 13.7, 5.5 Hz, 1 H; H_b–C(β)), 4.67 (ddd, *J* = 9.6, 8.3, 5.6 Hz, 1 H; H–C(α)), 7.37 (dd, *J* = 8.5, 2.1 Hz, 1 H; H–C(6)), 7.46 (dd, *J* = 8.4 Hz, ^5J(H,F) = 1.4 Hz, 1 H; H–C(5)), 7.62 (d, *J* = 2.1 Hz, 1 H; H–C(2)), 8.06 (d, *J* = 6.3 Hz, 2 H; H–C(3'',5'')), 8.56 (s, 1 H; H–C(5')), 8.82 (d, *J* = 6.3 Hz, 2 H; H–C(2'',6'')), 9.02 (d, *J* = 8.3 Hz, 1 H; HN–C(α)), 9.10 ppm (s, 1 H; NH). ^{13}C NMR (151 MHz, $(CD_3)_2SO$): δ = 15.57 and 15.64 (2 C; C(2,3) of cyclopropyl), 19.73 (C(1) of cyclopropyl), 35.85 (C(β)), 53.60 (C(α)), 112.81 (2 C; C(3'',5'')), 120.00 (q, ^1J(C,F) = 258.0 Hz; OCF_3), 120.55 (CN), 122.87 (C(5)), 125.50 (C(3)), 129.81 (C(6)), 131.64 (C(2)), 137.65 (C(5')), 139.11 (C(1)), 142.60 (C(4)), 144.58 and 144.63 (C(4''), C(4')), 151.62 (2 C; C(2'',6'')), 158.65 (O=*C*–C(4')), 171.58 ppm (O=*C*–C(α)). ^{19}F{^{1}H} NMR (355 MHz, $(CD_3)_2SO$): δ = –57.08 ppm. IR (ATR): $\tilde{\nu}$ = 3277 (w), 3030 (w), 2242 (w), 1650 (s), 1591 (m), 1534 (m), 1496 (m), 1344 (m), 1255 (s),

1216 (s), 1198 (s), 1165 (s), 1064 (m), 1020 (m), 965 (m), 870 (m), 827 (m), 708 (s), 666 cm^{-1} (m). HR-LC-MS: t_R = 2.72 min; *m/z* (%): 520.1136 (100, $[M + H]^+$, calcd for $C_{22}H_{18}{}^{35}ClF_3N_7O_3{}^+$: 520.1106).

3-Chloro-*N*-(1-cyanocyclopropyl)-4-*O*-(cyclobutylmethyl)-*N*$^{\alpha}$-[(2-(4-fluorophenyl)-2*H*-1,2,3-triazol-4-ylcarbonyl]-L-tyrosinamide (7b). A solution of **29b** (90 mg, 0.26 mmol) in DMF (2.5 mL) was treated with 2-(4-fluorophenyl)-2*H*-1,2,3-triazole-4-carboxylic acid (54 mg, 0.26 mmol), HATU (197 mg, 0.52 mmol), and *i*Pr_2NEt (158 µL, 0.91 mmol) according to GP-2. RP-HPLC (C18 column, 70:30 MeCN/H_2O + 0.05% Et_3N) **7b** (51 mg, 37%) as a yellow foam. R_f = 0.30 (SiO_2; heptane/EtOAc 1:1, UV 254 nm). m.p. 198–200 °C. $[\alpha]_D^{20}$ –25.1 (*c* 0.1, MeOH). ^{1}H NMR (600 MHz, $(CD_3)_2SO$): δ = 1.04–1.12 (m, 2 H; H_a–C(2,3) of cyclopropyl), 1.47–1.51 (m, 2 H; H_b–C(2,3) of cyclopropyl), 1.80–1.89 (m, 4 H; $H_2C(3)$, H_{trans}–C(2,4) of cyclobutyl), 1.99–2.05 (m, 2 H; H_{cis}–C(2,4) of cyclobutyl), 2.68 (hept., *J* = 7.4 Hz, 1 H; H–C(1) of cyclobutyl), 2.96 (dd, *J* = 13.8, 9.5 Hz, H_a–C(β)), 3.03 (dd, *J* = 13.8, 5.2 Hz, 1 H; H_b–C(β)), 3.95 (d, *J* = 6.4 Hz, 2 H; OCH_2), 4.60 (ddd, *J* = 9.5, 8.3, 5.3 Hz, 1 H; H–C(α)), 7.01 (d, *J* = 8.5 Hz, 1 H; H–C(5)), 7.17 (dd, *J* = 8.5, 2.2 Hz, 1 H; H–C(6)), 7.35 (d, *J* = 2.1 Hz, 1 H; H–C(2)), 7.49 (dd, *J* = 9.1 Hz, ^3J(H,F) = 8.4 Hz, 2 H; H–C(3'',5'')), 8.13 (dd, *J* = 9.1 Hz, ^4J(H,F) = 4.7 Hz, 2 H; H–C(2'',6'')), 8.45 (s, 1 H; H–C(5')), 8.78 (d, *J* = 8.3 Hz, 1 H; HN–C(α)), 9.09 ppm (s, 1 H; NH). ^{13}C NMR (151 MHz, $(CD_3)_2SO$): δ = 15.63 and 15.66 (2 C; C(2,3) of cyclopropyl), 18.07 (C(3) of cyclobutyl), 19.75 (C(1) of cyclopropyl), 24.18 (2 C; C(2,4) of cyclobutyl), 33.94 (C(1) of cyclobutyl), 35.75 (C(β)), 53.96 (C(α)), 72.24 (OCH_2), 113.76 (C(5)), 116.76 (d, ^2J(C,F) = 23.4 Hz; C(3'',5'')), 120.62 (CN), 120.97 (C(3)), 121.21 (d, ^3J(C,F) = 8.7 Hz, 2 C; C(2'',6'')), 128.96 (C(1)), 130.51 (C(2) or C(6)), 130.56 (C(2) or C(6)), 135.38 (d, ^4J(C,F) = 2.8 Hz; C(1'')), 136.53 (C(5')), 143.67 (C(4')), 152.69 (C(4)), 158.87 (O=C–C(4')), 161.66 (d, ^1J(C,F) = 245.8 Hz;

C(4’’)), 171.98 ppm (O=C–C(α)). ^{19}F{^{1}H} NMR (355 MHz, $(CD_3)_2SO$): δ = –113.18 ppm. IR (ATR): $\tilde{\nu}$ = 3415 (w), 3270 (w), 2936 (w), 2241 (w), 1692 (s), 1670 (s), 1539 (m), 1508 (s), 1321 (m), 1256 (m), 1222 (m), 1151 (m), 1062 (m), 971 (m), 837 (s), 818 (m), 771 (m), 637 cm^{-1} (m). HR-LC-MS: t_R = 3.56 min; *m/z* (%): 357.1719 (100, [*M* + H]$^+$, calcd for $C_{27}H_{27}{}^{35}ClFN_6O_3{}^+$: 537.1812).

3,4-Dichloro-*N*-(1-cyanocyclopropyl)-*N*$^{\alpha}$-[(2-(3,3-difluorocyclopropyl)-2*H*-1,2,3-triazol-4-ylcarbonyl]-L-phenylalaninamide (8c). A solution of **24h** (66 mg, 0.22 mmol) in DMF (2 mL) was treated with **21n** (45 mg, 0.22 mmol), HATU (168 mg, 0.44 mmol), and *i*Pr$_2$NEt (135 μL, 0.78 mmol) according to GP-2. MPLC (SiO_2; CH_2Cl_2/MeOH, gradient from 100: to 90:10 within 30 min) and MPLC (SiO_2; heptane/EtOAc, gradient from 100:0 to 0:100 within 30 min) gave **9c** (60 mg, 56%) as a white solid. R_f = 0.32 (SiO_2; CH_2Cl_2/MeOH 95:5, UV 254 nm). m.p. 180–183 °C. $[\alpha]_D^{20}$ –31.5 (*c* 0.1, MeOH). ^{1}H NMR (600 MHz, $(CD_3)_2SO$): δ = 1.02–1.11 (m, 2 H; H$_a$–C(2,3) of cyclopropyl), 1.46–1.52 (m, 2 H; H$_b$–C(2,3) of cyclopropyl), 3.01 (dd, *J* = 13.7, 9.6 Hz, 1 H; H$_a$–C(β)), 3.07 (dd, *J* = 13.7, 5.2 Hz, 1 H; H$_b$–C(β)), 3.21–3.29 (m, 2 H; H$_{trans}$–C(2’’,4’’)), 3.34–3.8 (m, 2 H; H$_{cis}$–C(2’’,4’’)), 4.61 (td, *J* ~ 9.4, 5.2 Hz, 1 H; H–C(α)), 5.28 (ttdd, *J* = 8.4, 6.8 Hz, ^4J(H,F) = 5.4 Hz, *J* = 1.7 Hz, 1 H; H–C(1’’)), 7.24 (dd, *J* = 8.3, 2.0 Hz, 1 H; H–C(6)), 7.51 (d, *J* = 8.2 Hz, 1 H; H–C(5)), 7.54 (d, *J* = 2.0 Hz, 1 H; H–C(2)), 8.22 (s, 1 H; H–C(5’)), 8.67 (d, *J* = 8.4 Hz, 1 H; HN–C(α)), 9.06 ppm (s, 1 H; NH). ^{13}C NMR (151 MHz, $(CD_3)_2SO$): δ = 15.63 (2 C; C(2,3) of cyclopropyl), 19.75 (C(1) of cyclopropyl), 35.85 (C(β)), 42.32 (dd, ^3J(C,F) = 24.3, 4.8 Hz; C(1’’)), 42.48 (dd, ^2J(C,F) = 24.0, 4.9 Hz) and 47.74 (dd, ^2J(C,F) = 18.2, ^3J(C,F) = 8.1 Hz; C(2’’,4’’)), 53.39 (C(α)), 118.40 (dd, ^1J(C,F) = 268.9, 269.0 Hz; C(3’’)) and 119.33 (d, ^1J(C,F) = 269.2 Hz; C(3’’)), 120.56 (CN), 129.09 (C(4)), 129.63 (C(6)), 130.22 (C(5)), 130.57 (C(3)), 131.24 (C(2)), 135.31 (C(5’)), 138.82 (C(1)), 142.57 (C(4’)), 159.05 (O=*C*–

C(4')), 171.72 ppm (O=*C*–C(α)). ^{19}F{^{1}H} NMR (355 MHz, $(CD_3)_2SO$): δ = –95.67 and –82.88 ppm (2 d, ^{2}J(F,F) = 195.7 Hz). IR (ATR): $\tilde{\nu}$ = 3295 (w), 2243 (w), 1679 (m), 1646 (m), 1543 (m), 1516 (m), 1472 (m), 1335 (s), 1302 (s), 1280 (m), 1251 (m), 1171 (m), 1033 (m), 952 (m), 886 (m), 868 (m), 680 cm^{-1} (m). HR-LC-MS: t_R = 2.91 min; *m/z* (%): 481.0772 (100, [*M* – H]$^-$, calcd for $C_{20}H_{17}{}^{35}Cl_2F_2N_6O_2^-$: 481.0764).

***N*-(1-Cyanocyclopropyl)-3-chloro-4-*O*-(trifluoromethyl)-L-tyrosinamide (12).** A solution of **13·HCl** (1.67 g, 5.21 mmol) in 1:1 dioxane/H_2O (40 mL) was treated with a 1 M NaOH aqueous solution (11.5 mL, 11.46 mmol) and Boc_2O (1.25 g, 5.73 mmol), at 23 °C under Ar. The mixture was stirred for 3 h at this temperature, before being concentrated *in vacuo*. The resulting aqueous solution was acifidied to pH ~ 5, and EtOAc (100 mL). The phases were separated, and the aqueous phase was extracted with EtOAc (3x). The combined organic layers were washed with brine, dried over Na_2SO_4, filtered, and evaporated. The crude product **14** (2 g, quant.) was obtained as an off-white foam, which was directly used in the next step. A solution of **14** (2 g, 5.21 mmol) in DMF (40 mL) was treated with 1-aminocyclopropanecarbonitrile hydrochloride (742 mg, 6.25 mmol), HATU (3.96 g, 10.4 mmol), and *i*Pr_2NEt (3.19 mL, 18.2 mmol), according to GP-2. MPLC (SiO_2; heptane/EtOAc, gradient from 100:0 to 0:100 within 40 min) yielded **15** (1.51 g, 65%) as a light yellow solid, which was directly used in the next step (R_f = 0.33 (SiO_2; heptane/EtOAc 1:1, $KMnO_4$)). A solution of **15** (1 g, 2.23 mmol) in formic acid (10 mL) was stirred for 2.5 h at 22 °C according to GP-3. Compound **12** (776 mg, quant.) was obtained as a yellow oil. $[\alpha]_D^{20}$ 33.1 (*c* 0.1, MeOH). ^{1}H NMR (600 MHz, $CDCl_3$): δ = 1.17–1.19 (m, 2 H; H–C(2,3) of cyclopropyl), 1.54–1.57 (m, 13 H; H–C(2,3) of cyclopropyl, NH_2, H_2O), 2.88 (dd, *J* = 14.0, 8.2 Hz, 1 H; H_a–C(β)), 3.18 (dd, *J* = 14.0, 4.4 Hz, 1 H; H_b–C(β)), 3.65 (dd, *J* = 8.1, 4.4 Hz, 1 H; H–C(α)), 7.14 (dd, *J* = 8.4, 2.2 Hz, 1 H; H–C(6)), 7.29 (dq, *J* = 8.4 Hz, ^{5}J(H,F) = 1.5 Hz, 1

H; H–C(5)), 7.32 (d, J = 2.1 Hz, 1 H; H–C(2)), 7.84 ppm (br. s, 1 H; NH). ^{13}C NMR (151 MHz, $CDCl_3$): δ = 16.68 and 16.70 (2 C; C(2,3) of cyclopropyl), 20.15 (C(1) of cyclopropyl), 39.69 (C(β)), 55.74 (C(α)), 119.91 (CN), 123.07 (C(5)), 127.77 (C(3)), 128.89 (C(6)), 131.77 (C(2)), 137.51 (C(1)), 144.41 (C(4)), 174.38 ppm (C=O), signal of OCF_3 hidden by noise. ^{19}F{^{1}H} NMR (377 MHz, $(CD_3)_2SO$): δ = –57.01 ppm. IR (ATR): $\tilde{\nu}$ = 3305 (br, w), 2241 (w), 1670 (m), 1494 (m), 1254 (s), 1217 (s), 1196 (s), 1167 (s), 1063 (m), 1045 (w), 931 (w), 894 (w), 828 (w), 668 cm^{-1} (w). HR-LC-MS: t_R = 1.70 min; *m/z* (%): 352.0741 (6), 350.0699 (35, [M + H]$^+$, calcd for $C_{14}H_{14}{}^{37}ClF_3N_3O_2{}^+$: 350.0718), 348.0724 (100, [M + H]$^+$, calcd for $C_{14}H_{14}{}^{35}ClF_3N_3O_2{}^+$: 348.0721).

Ethyl 1*H*-1,2,3-Triazole-4-carboxylate (16).[39] On a Vapourtec R2+/R4 flow system equipped with three 10 mL PTA reactor coils and a 250 psi back pressure regulator, neat ethyl propiolate and trimethylsilyl azide were injected *via* 2 mL loops. The flow rate was set to 0.5 mL min^{-1}, providing a total residence time of 30 min. The system was heated to 140 °C and injections were performed every 40 min. Acetonitrile was used as a carrier solvent at a flow rate of 1.0 mL min^{-1}. In total, 5 injections were performed and the total mixture coming out of the reactor was collected. Acetonitrile was evaporated (the collector of the rotary evaporator was filled with sat. aq. $NaHCO_3$ solution to neutralize any potentially formed HN_3). A solution of the residue in EtOAc was washed with brine (3x), dried over Na_2SO_4, filtered, and evaporated. The crude product was stirred in a minimal amount of Et_2O. Filtration and drying gave **16** (8.65 g, 81%) as a white solid. R_f = 0.19 (SiO_2; heptane/EtOAc 1:1, $KMnO_4$). m.p. 113–118 °C ([39]: 125–127 °C). ^{1}H NMR (600 MHz, $CDCl_3$): δ = 1.42 (t, J = 7.2 Hz, 3 H; CH_3), 4.47 (q, J = 7.1 Hz, 2 H; OCH_2), 8.28 ppm (H–C(5)). ^{13}C NMR (151 MHz, $CDCl_3$): δ = 14.39 (CH_3), 61.95 (OCH_2), 132–137 (br, C(5)), 139.51 (br, C(4)), 161.09 ppm (C=O). IR (ATR): $\tilde{\nu}$ = 3153 (br, w), 2995 (w), 1705 (s),

1532 (w), 1471 (m), 1455 (m), 1401 (w), 1374 (m), 1329 (s), 1241 (m), 1231 (w), 1198 (s), 1114 (m), 1044 (m), 1025 (s), 886 (w), 862 (m), 839 (s), 779 (s), 695 cm^{-1} (s). HR-EI-MS: *m/z* (%): 141.053 (100, $[M]^+$, calcd for $C_5H_7N_3O_2^+$: 141.0533).

Ethyl 2-(6-Fluoropyridin-3-yl)-2*H*-triazole-4-carboxylate (19f). A solution of 5-bromo-2-fluoropyridine (500 mg, 2.84 mmol) in toluene (3 mL) was treated with **16** (481 mg, 3.41 mmol), Me_4*t*BuXPhos (27 mg, 0.06 mmol), $[Pd_2(dba)_3]$ (26 mg, 0.03 mmol), and K_3PO_4 (5.68 mmol) according to GP-4. MPLC (SiO_2; heptane/EtOAc, gradient from 100:0 to 50:50 within 30 min) gave **19f** (10 mg, 2%) as a white solid. R_f = 0.75 (SiO_2; heptane/EtOAc 1:1, UV 254 nm). m.p. 108–110 °C. ^{1}H NMR (600 MHz, $CDCl_3$): δ = 1.45 (t, J = 7.1 Hz, 3 H; CH_3), 4.49 (q, J = 7.1 Hz, 2 H; OCH_2), 7.11 (ddd, J = 8.9 Hz, ^3J(H,F) = 3.4 Hz, J = 0.7 Hz, 1 H; H–C(5')), 8.27 (s, 1 H; H–C(5)), 8.55 (ddd, J = 8.8 Hz, ^4J(H,F) = 6.6 Hz, J = 2.8 Hz, 1 H; H–C(4')), 9.04 ppm (ddd, J = 2.9 Hz, ^4J(H,F) = 1.4 Hz, J = 0.6 Hz, 1 H; H–C(2')). ^{13}C NMR (151 MHz, $CDCl_3$): δ = 14.44 (CH_3), 62.07 (OCH_2), 110.32 (d, ^2J(C,F) = 39.4 Hz; C(5')), 132.67 (d, ^3J(C,F) = 8.5 Hz; C(4')), 134.27 (d, ^4J(C,F) = 5.3 Hz; C(3')), 138.56 (C(5)), 139.27 (d, ^3J(C,F) = 16.5 Hz; C(2')), 142.10 (C(4)), 160.31 (C=O), 162.88 ppm (d, ^1J(C,F) = 241.9 Hz; C(6')). ^{19}F{^{1}H} NMR (377 MHz, $CDCl_3$): δ = –67.07 ppm. IR (ATR): $\tilde{\nu}$ = 3124 (w), 3083 (w), 2987 (w), 2941 (w), 1724 (s), 1612 (m), 1603 (m), 1514 (m), 1487 (m), 1463 (m), 1446 (m), 1432 (m), 1402 (w), 1351 (w), 1330 (m), 1297 (m), 1270 (w), 1255 (m), 1233 (s), 1221 (m), 1128 (s), 1096 (m), 1022 (s), 999 (s), 972 (s), 941 (m), 896 (m), 860 (w), 846 (m), 834 (s), 778 (m), 739 (m), 673 (m), 656 (m), 638 cm^{-1} (m). HR-ESI-MS: *m/z* (%): 238.0804 (14), 237.0777 (100, $[M + H]^+$, calcd for $C_{10}H_{10}FN_4O_2^+$: 237.0782).

Ethyl 2-(Pyridin-4-yl)-2*H*-1,2,3-triazole-4-carboxylate (19h). A solution of **16** (500 mg, 3.54 mmol) in DMF (20 mL) was treated with $Cu(OAc)_2$ (1.29 g, 7.09 mmol), (pyridin-4-

yl)boronic acid (871 mg, 7.09 mmol), and pyridine (573 µL, 7.09 mmol) according to GP-5. MPLC (SiO_2; heptane/EtOAc, gradient from 100:0 to 50:50 within 30 min) gave **19h** (8 mg, 1%) as a white solid. R_f = 0.24 (SiO_2; heptane/EtOAc 1:1, UV 254 nm). m.p. 108–110 °C. ^{1}H NMR (600 MHz, $CDCl_3$): δ = 1.45 (t, J = 7.1 Hz, 3 H; CH_3), 4.49 (q, J = 7.1 Hz, 2 H; OCH_2), 8.08 (br d, J = 6.3 Hz, 2 H; H–C(3',5')), 8.29 (s, 1 H; H–C(5)), 8.78 ppm (br d, J = 6.4 Hz, 2 H; H–C(2',6')). ^{13}C NMR (151 MHz, $CDCl_3$): δ = 14.43 (CH_3), 62.14 (OCH_2), 113.48 (2 C; C(3',5')), 138.88 (C(5)), 142.54 (C(4)), 145.38 (C(4')), 151.50 (2 C; C(2',6')), 160.23 ppm (C=O). IR (ATR): $\tilde{\nu}$ = 3109 (w), 2998 (w), 2914 (w), 1721 (s), 1595 (m), 1585 (m), 1513 (m), 1504 (m), 1490 (m), 1480 (w), 1447 (m), 1422 (m), 1344 (w), 1325 (m), 1243 (s), 1224 (m), 1217 (m), 1154 (m), 1112 (m), 1090 (m), 1032 (m), 1015 (s), 993 (m), 969 (m), 887 (m), 839 (s), 826 (s), 779 (s), 709 (s), 672 cm^{-1} (s). HR-ESI-MS: *m/z* (%): 220.09064 (14), 219.08866 (100, $[M + H]^+$, calcd for $C_{10}H_{11}N_4O_2^+$: 219.0877).

Ethyl 2-(3,3-Difluorocyclobutyl)-2*H*-triazole-4-carboxylate (19n). A solution of **16** (300 mg, 2.13 mmol) in toluene (15 mL) was treated with 3,3-difluorocyclobutanol (345 mg, 3.19 mmol) and 2-(tributylphosphoranylidene)acetonitrile (1.11 mL, 4.25 mmol) according to GP-6. MPLC (SiO_2; heptane/EtOAc, gradient from 100:0 to 60:40 within 30 min) gave **19n** (37 mg, 8%) as a white solid. R_f = 0.72 (SiO_2; heptane/EtOAc 1:1, UV 254 nm). ^{1}H NMR (600 MHz, $CDCl_3$; assignments based on HSQC, NOESY and ^{15}N-HMBC spectra): δ = 1.41 (t, J = 7.1 Hz, 3 H; CH_3), 3.19–3.27 (m, 2 H; H_{trans}–C(2',4')), 3.32–3.41 (m, 2 H; H_{cis}–C(2',4')), 4.44 (q, J = 7.1 Hz, 2 H; OCH_2), 5.14 (ddddd, J = 15.8, 8.6, 7.5, 4.8, 1.3 Hz, 1 H; H–C(1')), 8.09 ppm (s, 1 H; H–C(5)). ^{13}C NMR (151 MHz, $CDCl_3$; assignments based on a HSQC spectrum): δ = 14.44 (CH_3), 43.37 (dd, ^2J(C,F) = 24.6 Hz, 2 C; C(2',4')), 49.02 (dd, ^3J(C,F) = 20.1, 5.1 Hz; C(1')), 61.76 (OCH_2), 137.45 (C(5)), 140.71 (C(4)), 160.55 ppm (C=O). ^{19}F{^{1}H} NMR (355 MHz,

$CDCl_3$): δ = –99.30 (d, ^2J(F,F) = 200.3 Hz), –84.41 ppm (d, ^2J(F,F) = 200.3 Hz). IR (ATR): $\tilde{\nu}$ = 3156 (w), 3126 (w), 2986 (w), 2942 (w), 1726 (s), 1471 (m), 1395 (m), 1329 (m), 1303 (m), 1272 (m), 1250 (s), 1225 (s), 1161 (s), 1143 (s), 1113 (m), 1032 (m), 901 (m), 885 (m), 863 (m), 811 (s), 781 (s), 735 (s), 711 cm^{-1} (s). HR-LC-MS: t_R = 1.92 min; *m/z* (%): 231.082 (100, $[M]^+$, calcd for $C_9H_{11}F_2N_3O_2^+$: 231.081).

2-(Pyridin-4-yl)-2*H*-1,2,3-triazole-4-carboxylic Acid (21h). A solution of **19h** (37 mg, 0.17 mmol) in THF/MeOH/H_2O 2:2:1 (2.5 mL) was treated with LiOH (8 mg, 0.34 mmol) according to GP-1. Acid **21h** (32 mg, 99%) was obtained as a white solid. ^{1}H NMR (600 MHz, $(CD_3)_2SO$): δ = 8.18 (br d, *J* = 6.7 Hz, 2 H; H–C(3',5')), 8.69 (s, 1 H; H–C(5)), 8.88 (br d, *J* = 6.6 Hz, 2 H; H–C(2',6')), 13.6–14.2 ppm (br s, 1 H; COOH). ^{13}C NMR (151 MHz, $(CD_3)_2SO$): δ = 113.69 (2 C; C(3',5')), 139.93 (C(5)), 143.53 C(4)), 145.87 (C(4')), 149.78 (2 C; C(2',6')), 160.75 ppm (C=O). IR (ATR): $\tilde{\nu}$ = 3400–2500 (w), 1706 (m), 1633 (s), 1615 (s), 1543 (m), 1503 (m), 1337 (m), 1317 (m), 1245 (m), 1209 (m), 1141 (m), 1016 (m), 953 (m), 841 (s), 817 (s), 788 (s), 757 (s), 713 cm^{-1} (m). HR-LC-MS: t_R = 0.34 min; *m/z* (%): 191.0570 (100, $[M + H]^+$, calcd for $C_8H_7N_4O_2^+$: 191.0564).

2-(3,3-Difluorocyclobutyl)-2*H*-1,2,3-triazole-4-carboxylic Acid (21n). A solution of **19n** (125 mg, 0.54 mmol) in THF/MeOH/H_2O 2:2:1 (2.5 mL) was treated with LiOH (26 mg, 1.08 mmol) according to GP-1. Acid **21n** (95 mg, 86%) was obtained as a white solid. M.p. 157–161 °C. ^{1}H NMR (600 MHz, $CDCl_3$): δ = 3.17–3.27 (m, 2 H; H_{trans}–C(2',4')), 3.30–3.39 (m, 2 H; H_{cis}–C(2',4')), 5.31 (ttdd, *J* = 8.5, 6.8 Hz, ^4J(H,F) = 5.4 Hz, *J* = 1.7 Hz, 1 H; H–C(1')), 8.29 (s, 1 H; H–C(5)), 13.43 ppm (br s, 1 H; COOH). ^{13}C NMR (151 MHz, $CDCl_3$): δ = 42.38 (dd, ^2J(C,F) = 23.7, 23.7 Hz, 2 C; C(2',4')), 47.91 (dd, ^3J(C,F) = 18.0, 8.4 Hz, 2 C; C(1')), 47.85 (d, ^3J(C,F) = 8.4 Hz) and 47.97 (d, ^3J(C,F) = 8.3 Hz) (C(1')), 118.39 (dd, ^1J(C,F) = 280.6, 269.2 Hz; C(3')),

137.36 (C(5)), 140.63 (C(4)), 161.25 ppm (C=O). ^{19}F{^{1}H} NMR (355 MHz, $CDCl_3$): δ = –95.56 (d, ^{2}J(C,F) = 195.8 Hz), –83.03 ppm (d, ^{2}J(C,F) = 195.8 Hz). IR (ATR): $\tilde{\nu}$ = 3134–2549 (br, COOH), 1693 (s), 1518 (m), 1403 (m), 1368 (m), 1298 (s), 1249 (s), 1232 (s), 1218 (s), 1171 (s), 1161 (s), 1103 (s), 966 (m), 856 (m), 897 (s), 761 (s), 711 (s), 683 cm^{-1} (m). HR-LC-MS (negative mode): t_R = 1.37 min; *m/z* (%): 202.0441 (100, [*M* – H]$^-$, calcd for $C_7H_6F_2N_3O_2^-$: 202.0434).

N^{α}-[(*tert*-Butoxy)carbonyl]-*N*-(1-cyanocyclopropyl)-3,4-dichloro-L-phenylalaninamide (23h). A solution of N^{α}-[(*tert*-Butoxy)carbonyl]-3,4-dichloro-L-phenylalanine (319 mg, 0.95 mmol) in DMF (10 mL) was treated with 1-aminocyclopropanecarbonitrile hydrochloride (136 mg, 1.15 mmol), HATU (726 mg, 1.91 mmol), and *i*Pr_2NEt (583 µL, 3.34 mmol) according to GP-2. MPLC (SiO_2; heptane/EtOAc, gradient from 100:0 to 0:100 within 30 min) gave **23h** (260 mg, 68%) as a white solid. R_f = 0.42 (SiO_2; heptane/EtOAc 1:1, UV 254 nm). m.p. 164–168 °C. $[\alpha]_D^{20}$ +8.3 (*c* 1.0, MeOH). ^{1}H NMR (600 MHz, $CDCl_3$): δ = 1.10–1.17 (m, 2 H; H_a–C(2,3) of cyclopropyl), 1.42 (s, 9 H; CMe_3), 1.48–1.56 (m, 2 H; H_b–C(2,3) of cyclopropyl), 2.96 (dd, *J* = 13.9, 7.1 Hz, 1 H; H_a–C(β)), 3.06 (dd, *J* = 13.9, 7.1 Hz, 1 H; H_b–C(β)), 4.23 (q, *J* = 7.3 Hz, 1 H; H–C(α)), 5.08 (br s, 1 H; HN–C(α)), 6.92 (br s, 1 H; NH), 7.06 (dd, *J* = 8.2, 2.1 Hz, 1 H; H–C(6)), 7.28 (d, *J* = 2.1 Hz, 1 H; H–C(2)), 7.38 ppm (d, *J* = 8.2 Hz, 1 H; H–C(5)). ^{13}C NMR (151 MHz, $CDCl_3$): δ = 16.81 and 16.94 (2 C; C(2,3) of cyclopropyl), 20.47 (C(1) of cyclopropyl), 28.36 (C*Me*$_3$), 37.16 (C(β)), 55.34 (C(α)), 81.28 (*C*Me_3), 119.61 (CN), 128.94 (C(6)), 130.86 (C(5)), 131.35 (C(2)), 131.50 (C(4)), 132.78 (C(3)), 136.63 (C(1)), 155.79 (O–C=O), 171.95 ppm (O=*C*–C(α)). IR (ATR): $\tilde{\nu}$ = 3326 (w), 3295 (w), 3026 (w), 2973 (w), 2934 (w), 2235 (w), 1668 (s), 1519 (s), 1468 (m), 1422 (m), 1389 (m), 1313 (m), 1284 (m), 1270 (m), 1252 (m), 1224 (m), 1208 (m), 1161 (s), 1145 (m), 1136 (m), 1054 (m), 1032 (m), 1025 (m),

1017 (m), 953 (w), 935 (w), 889 (w), 805 (w), 741 (m), 659 cm^{-1} (m). HR-ESI-MS: *m/z* (%): 298.049 (100, $[M + H - Boc]^+$, calcd for $C_{13}H_{14}{}^{35}Cl_2N_3O^+$: 298.0508).

***N*-(1-Cyanocyclopropyl)-3,4-dichloro-L-phenylalaninamide (24h).** A solution of **23h** (240 mg, 0.6 mmol) in formic acid (3 mL) was stirred for 5 h according to GP-3. Evaporation gave **24h** (168 mg, 94%) as a colorless oil. $[\alpha]_D^{20}$ +34.9 (*c* 1.0, MeOH). ^{1}H NMR (600 MHz, $CDCl_3$): δ = 1.15–1.23 (m, 2 H; H_a–C(2,3) of cyclopropyl), 1.50 (br s, 2 H; NH_2), 1.54–1.57 (m, 2 H; H_b–C(2,3) of cyclopropyl), 2.86 (dd, *J* = 14.0, 8.1 Hz, 1 H; H_a–C(β)), 3.13 (dd, *J* = 14.0, 4.4 Hz, 1 H; H_b–C(β)), 3.62 (dd, *J* = 8.1, 4.4 Hz, 1 H; H–C(α)), 7.03 (dd, *J* = 8.2, 2.1 Hz, 1 H; H–C(6)), 7.29 (d, *J* = 2.1 Hz, 1 H; H–C(2)), 7.40 (d, *J* = 8.2 Hz, 1 H; H–C(5)), 7.84 ppm (br s, 1 H; NH). ^{13}C NMR (151 MHz, $CDCl_3$): δ = 16.67 and 16.74 (2 C; C(2,3) of cyclopropyl), 20.15 (C(1) of cyclopropyl), 39.71 (C(β)), 55.71 (C(α)), 119.93 (CN), 128.93 (C(6)), 130.91 (C(5)), 131.36 (C(2)), 131.42 (C(4)), 132.87 (C(3)), 137.40 (C(1)), 174.61 ppm (C=O). IR (ATR): $\tilde{\nu}$ = 3300 (br, w), 3021 (w), 2928 (w), 2240 (w), 1668 (s), 1593 (w), 1560 (w), 1471 (s), 1425 (m), 1395 (m), 1301 (m), 1208 (w), 1132 (m), 1031 (m), 900 (m), 816 (m), 730 (m), 707 (m), 683 cm^{-1} (m). HR-ESI-MS: *m/z* (%): 302.0464 (14, $[M + H]^+$, calcd for $C_{13}H_{14}{}^{37}Cl_2N_3O^+$: 302.0491), 300.0490 (71, $[M + H]^+$, calcd for $C_{13}H_{14}{}^{37}Cl^{35}ClN_3O^+$: 300.0499), 299.0545 (17), 298.05215 (100, $[M + H]^+$, calcd for $C_{13}H_{14}{}^{35}Cl_2N_3O^+$: 298.0508).

***N*-[(*tert*-Butoxy)carbonyl]-3-chloro-4-*O*-(cyclobutylmethyl)-L-tyrosine Cyclobutylmethyl Ester (26b).** A solution of dicyclohexylamine N^{α}-[*tert*-(butoxy)carbonyl]-3-chloro-L-tyrosine (500 mg, 1.01 mmol) in DMF (5 mL) was treated with (bromomethyl)cyclobutane (392 µL, 3.52 mmol) and Cs_2CO_3 (1.15 g, 3.52 mmol) according to GP-7. MPLC (SiO_2; heptane/EtOAc, gradient from 100:0 to 50:50 within 30 min) gave **26b** (318 mg, 70%) as a colorless oil. R_f = 0.78 (SiO_2; heptane/EtOAc 1:1; UV 254 nm). $[\alpha]_D^{20}$ 30.9 (*c* 0.1, $CHCl_3$). ^{1}H NMR (600 MHz,

$CDCl_3$): δ = 1.43 (br s, 9 H; CMe_3), 1.69–1.75 (m, 2 H; CH_2), 1.83–2.00 (m, 6 H; $H_2C(3')$, $H_2C(3'')$), 2.02–2.07 (m, 2 H; CH_2), 2.10–2.17 (m, 2 H; CH_2), 2.59 (hept, J = 7.5 Hz, 1 H; CH), 2.80 (dq, J = 14.3, 7.8, 7.4 Hz, 1 H; CH), 2.97 (dd, J = 14.0, 5.9 Hz, 1 H; H_a–C(β)), 3.03 (dd, J = 14.0, 6.0 Hz, 1 H; H_b–C(β)), 3.96 (d, J = 6.3 Hz, 2 H; OCH_2), 4.08 (d, J = 6.8 Hz, 2 H; OCH_2), 4.52 (q, J ~ 6.6 Hz, 1 H; H–C(α)), 4.99 (d, J = 8.2 Hz, 1 H; HN–C(α)), 6.83 (d, J = 8.3 Hz, 1 H; H–C(5)), 6.96 (dd, J = 8.4, 2.2 Hz, 1 H; H–C(6)), 7.12 ppm (d, J = 2.2 Hz, 1 H; H–C(2)). ^{13}C NMR (151 MHz, $CDCl_3$): δ = 18.53 and 18.74 (2 C; C(3',3'')), 24.84, 24.91 (3 C; C*Me₃*), 28.46, 34.03, 34.74, 37.47 (C(β)), 54.59 (C(α)), 69.42 (OCH_2), 73.26 (OCH_2), 80.09 (CMe_3), 113.81 (C(5)), 123.12 (C(3)), 128.52 (C(6)), 129.22 (C(1)), 131.20 (C(2)), 153.94 (C(4)), 155.16 (O=C–O), 171.99 ppm (O=*C*–C(α)). IR (ATR): $\tilde{\nu}$ = 2976 (w), 2937 (w), 2864 (w), 1712 (s), 1499 (s), 1365 (m), 1283 (m), 1254 (s), 1161 (s), 1060 (s), 1008 (s), 804 (m), 778 cm^{-1} (m). HR-LC-MS: t_R = 4.23 min; *m/z* (%): 352.168 (100, [M – CH_2=CMe_2 – CO_2 + H]$^+$, calcd for $C_{19}H_{27}{}^{35}ClNO_3{}^+$: 352.1674).

N^{α}-[(*tert*-Butoxy)carbonyl]-3-chloro-*N*-(1-cyanocyclopropyl)-4-*O*-(cyclobutylmethyl)-L-tyrosinamide (28b). A solution of **26b** (300 mg, 0.66 mmol) in THF/MeOH/H_2O 2:2:1 (5 mL) was treated with LiOH (32 mg, 1.33 mmol) according to GP-1. Acid **27b** (255 mg, 80%) was obtained as a colorless oil, which was directly used in the next step. A solution of **27b** (255 mg, 0.66 mmol) in DMF (10 mL) was treated with 1-aminocyclopropanecarbonitrile hydrochloride (79 mg, 0.66 mmol), HATU (505 mg, 1.33 mmol), and *i*Pr_2NEt (406 µL, 2.33 mmol) according to GP-2. MPLC (SiO_2; heptane/EtOAc, gradient from 100:0 to 0:100 within 30 min) gave **28b** (150 mg, 50%) as a white solid. R_f = 0.43 (SiO_2; heptane/EtOAc 1:1, UV 254 nm). m.p. 135–137 °C. $[\alpha]_D^{20}$ 1.2 (c 0.1, $CHCl_3$). ^{1}H NMR (600 MHz, $CDCl_3$): δ = 1.08–1.16 (m, 2 H; H_a–C(2,3) of cyclopropyl), 1.43 (s, 9 H; CMe_3), 1.49–1.53 (m, 2 H; H_b–C(2,3) of cyclopropyl), 1.90–1.99 (m,

4 H; $H_2C(3')$, H_{trans}–C(2',4')), 2.11–2.17 (m, 2 H; H_{cis}–C(2',4')), 2.80 (hept., J = 7.8 Hz, 1 H; H–C(1')), 2.94 (dd, J = 13.9, 7.5 Hz, H_a–C(β)), 3.00 (dd, J = 13.9, 6.4 Hz, 1 H; H_b–C(β)), 3.96 (d, J = 6.3 Hz, 2 H; OCH_2), 4.17 (br q, J = 7.3 Hz, 1 H; H–C(α)), 5.00 (br s, 1 H; HN–C(α)), 6.56 (br s, 1 H; NH), 6.86 (d, J = 8.4 Hz, 1 H; H–C(5)), 7.02 (dd, J = 8.2, 2.2 Hz, 1 H; H–C(6)), 7.17 ppm (d, J = 2.2 Hz, 1 H; H–C(2)). ^{13}C NMR (151 MHz, $CDCl_3$): δ = 16.90 and 16.98 (2 C; C(2,3) of cyclopropyl), 18.73 (C(1) of cyclopropyl), 20.41 (C(3')), 24.91 (2 C; C(2',4')), 28.38 (3 C; C*Me₃*), 34.72 (C(1')), 37.09 (C(β)), 55.79 (C(α)), 73.26 (OCH_2), 81.01 (CMe$_3$), 114.07 (C(5)), 119.59 (CN), 123.31 (C(3)), 128.73 (C(6)), 129.08 (C(1)), 130.96 (C(2)), 154.09 (O=C–O), 155.68 (C(4)), 172.16 ppm (O=C–C(α)). IR (ATR): $\tilde{\nu}$ = 3339 (w), 3297 (w), 2936 (w), 2235 (w), 1668 (s), 1517 (s), 1381 (m), 1282 (m), 1163 (m), 1062 (m), 1024 (m), 1011 (m), 990 (m), 949 (m), 819 (m), 804 (m), 645 cm^{-1} (m). HR-LC-MS: t_R = 3.38 min; *m/z* (%): 448.1981 (100, [M + H]$^+$, calcd for $C_{23}H_{31}{}^{35}ClN_3O_4{}^+$: 448.1998).

3-Chloro-*N*-(1-cyanocyclopropyl)-4-*O*-(cyclobutylmethyl)-L-tyrosinamide (29b). A solution of **28b** (150 mg, 0.34 mmol) in formic acid (1.3 mL) was stirred for 2 h at 22 °C according to GP-3. Evaporation gave **29b** (100 mg, 86%) as a colorless oil. $[\alpha]_D^{20}$ –62.8 (c 0.1, $CHCl_3$). ^{1}H NMR (600 MHz, $CDCl_3$): δ = 1.17–1.22 (m, 2 H; H_a–C(2,3) of cyclopropyl), 1.43 (br s, 2 H; NH_2), 1.52–1.57 (m, 2 H; H_b–C(2,3) of cyclopropyl), 1.89–2.01 (m, 4 H; $H_2C(3')$, H_{trans}–C(2',4')), 2.11–2.18 (m, 2 H; H_{cis}–C(2',4')), 2.81 (dd, J = 14.0, 8.0 Hz, 1 H; H_a–C(β)), 2.81 (hidden hept., 1 H; H–C(1')), 3.06 (dd, J = 14.0, 4.5 Hz, 1 H; H_b–C(β)), 3.58 (dd, J = 8.0, 4.5 Hz, 1 H; H–C(α)), 3.97 (d, J = 6.4 Hz, 2 H; OCH_2), 6.87 (d, J = 8.4 Hz, 1 H; H–C(5)), 7.02 (dd, J = 8.4, 2.2 Hz, 1 H; H–C(6)), 7.17 (d, J = 2.2 Hz, 1 H; H–C(2)), 7.80 ppm (br s, 1 H; NH). ^{13}C NMR (151 MHz, $CDCl_3$): δ = 16.68 and 16.75 (2 C; C(2,3) of cyclopropyl), 18.73 (C(3')), 20.10 (C(1) of cyclopropyl), 24.91 (2 C; C(2',4')), 34.73 (C(1')), 39.49 (C(β)), 55.91 (C(α)),

73.29 (OCH_2), 114.10 (C(5)), 120.00 (CN), 123.33 (C(3)), 128.67 (C(6)), 129.89 (C(1)), 131.04 (C(2)), 154.01 (C(4)), 175.03 ppm (C=O). IR (ATR): $\tilde{\nu}$ = 3304 (w), 2934 (w), 2862 (w), 2240 (w), 1670 (m), 1498 (s), 1425 (m), 1283 (m), 1254 (s), 1060 (s), 1007 (m), 990 (m), 804 cm^{-1} (m). HR-LC-MS: t_R = 1.93 min; *m/z* (%): 348.1488 (100, $[M + H]^+$, calcd for $C_{18}H_{23}{}^{35}ClN_3O_2{}^+$: 348.1473).

Determination of RD and hCatL Activity. The inhibitory constants (K_i) of the ligands against RD and hCatL were calculated from the IC_{50} values using the Cheng-Prusoff equation.[69] The IC_{50} values were determined in a fluorescence-based assay according to previously published procedures.[56,57]

***In Vitro* Evaluation.** The *in vitro* activities against *T. b. rhodesiense*, *T. cruzi*, *L. donovani* and *P. falciparum* as well as the cytotoxicity assessment in L6 cells were determined as reported elsewhere.[70] The following strains and parasite forms were used: *T. b. rhodesiense*, STIB900, trypomastigotes; *T. cruzi*, Tulahuen C2C4 (LacZ), amastigotes; *L. donovani*, MHOM-ET-67/L82, axenically grown amastigotes; *P. falciparum*, NF54, erythrocytic forms; L6 cells, rat skeletal myoblasts.

Reversibility of Drug Effect. Medium (50 µL) was added to each well of a 96-V-well microtiter plate. Serial drug dilutions of eleven 3-fold dilution steps were prepared. Then $1x10^4$ bloodstream forms of *T. b. rhodesiense* STIB 900 in 50 µL were added to each well and the plate incubated at 37 °C under a 5% CO_2 atmosphere for a specified time (24 h, 48 h). At the designated time the plate was centrifuged at 2000 RCF for 3 min, to sediment the parasites. 50 µL of the supernatant were aspirated, and 200 µL of warmed medium were added. The plate was centrifuged again and 200 µL of supernatant were aspirated. This wash step was repeated 3 more

times. After the final wash, 200 μL of supernatant were removed. Thereafter, 50 μL of medium were added in the wells to the remaining 50 μL, to get a total volume of 100 μL per well.

Parasite Recovery: Triplicate plates were made for each time point into 96-well flat-bottomed plates. 10 μL of the V-bottomed plate suspension to the corresponding wells of a flat-bottomed plate was added, and the volume was completed to 100 μL per well with medium. The plates were then incubated for 72 h at 37 °C / 5% CO_2. 10 μL Alamar Blue® (resazurin, 12.5 mg in 100 mL double-distilled water) were then added to each well and incubation continued for another 2–4 h.[62] The plates were read on a fluorimeter using an excitation wavelength of 536 nm and an emission wavelength of 588 nm. The IC_{50} values were calculated by linear regression from the sigmoidal dose inhibition curves.[71] Melarsoprol was used as control.

***In Vivo T. b. rhodesiense* (STIB900) Acute Mouse Model.** The STIB900 *T. b. rhodesiense* acute mouse model mimics the first stage of the disease. Two female NMRI mice were used per experimental group. Each mouse was inoculated i.p. with 10^4 bloodstream forms of STIB900, respectively. Heparinized blood from a donor mouse with approximately $5x10^6$/mL parasitaemia was suspended in PSG to obtain a trypanosome suspension of 1×10^5/mL. Each mouse was injected with 0.25 mL. Compounds were formulated in 100% DMSO, and diluted 10-fold in distilled water. Compound treatment was initiated 1 day post-infection and administered orally on three consecutive days in a volume of 0.1 mL/10 g. Four mice served as infected-untreated controls. They were not injected with the vehicle alone since we have established in our labs that these vehicles do not affect parasitaemia or the mice. The tail blood of all mice was checked for parasitaemia reduction (versus untreated control mice) at 24 h after the final dose of the compounds. Mice were euthanized after 24 h if the parasitaemia reduction was not > 90%. The tail blood of aparasitaemic mice was examined twice per week for 30 days post infection, and

mice with detected parasitaemia relapses were euthanized. The mice that remained aparasitaemic until day 30 were considered as cured. *In vivo* efficacy studies in mice were conducted at the Swiss Tropical and Public Health Institute (Basel) (License number 2813) according to the rules and regulations for the protection of animal rights ("Tierschutzverordnung") of the local Swiss "Bundesamt für Veterinärwesen". They were approved by the veterinary office of Canton Basel-Stadt, Switzerland.

DMPK Parameters: LogD$_{7.4}$ Determination. Distribution coefficients were determined in a CAMDIS© (CArrier Mediated DIstribution System, EP2005102211A) assay, as previously reported.[60]

Permeability. The permeability was determined *via* PAMPA (Parallel Artificial Membrane Permeation Assay), as previously reported.[72]

Solubility. The solubility was determined in a lyophilisation solubility assay (LYSA), as previously reported.[61]

Stability in Mouse Microsomes. The stability was determined in a NADH-dependent assay as previously reported.[61]

CYP Inhibition. The inhibition of the cytochromes P450 (CYP) 2C9, 2D6, and 3A4 was assessed using human liver microsomes and CYP-selective substrate metabolism reactions, as previously described.[73]

Mouse PK. All studies were conducted with the approval of the local veterinary authority in strict adherence to the Swiss federal regulations on animal protection and to the rules of the Association for Assessment and Accreditation of Laboratory Animal Care International (AAALAC). Male adult C57BL/6J mice were administered the test compounds orally (gavage), or intravenously (bolus). Test compounds were dissolved in *N*-methylpyrrolidinone and 40%

(v/v) aqueous hydroxypropyl-γ-cyclodextrine (30/70 v/v) for intravenous (i.v.) administration or micronized to suspensions in water (pH 6) containing hydroxymethylcellulose (1.25% w/v) and dioctyl sulfosuccinate (0.1% w/v) using a mixer mill for oral gavage. Blood was collected into K_2EDTA coated polypropylene tubes at 5 min (i.v. only), 15 min, 30 min, 1 h, 2 h, 4 h, and 8 h post dose sublingually or terminally by cardiac puncture under deep anesthesia with 5% isoflurane in pure oxygen. Blood was stored on ice and plasma was prepared within 30 min by centrifugation at 3000 × g for 5 min at 4 °C and frozen immediately. All plasma samples were stored at −20 °C. Compound concentrations in plasma were determined high performance liquid chromatography–tandem mass spectrometry (LC–MS/MS). Pharmacokinetic parameters were calculated by non-compartmental analysis using an in-house built software package.

MDR1-Mediated Transport. Porcine kidney epithelial cells LLC-PK1 stably transfected with Abcb1a (Mdr1a, mouse P-gp) or ABCB1 (MDR1, human P-gp) were provided by Dr. A. Schinkel at The Netherlands Cancer Institute (Amsterdam, The Netherlands) and used under license agreement. Cells were cultivated in Medium 199 with stable glutamine and phenol red, supplemented with 10% fetal calf serum, 100 IU/mL–100/ng/mL penicillin/streptomycin and 100 ng/mL colchicine at 37 °C in a humidified 5% CO_2 cell culture incubator and seeded at low density on permeable Costar1 inserts (0.33 cm^2 area, pore size 3.0 mm).

Transport measurements were performed on day 4 after seeding. The tightness of the cell monolayer was controlled with the permeability of an extracellular marker (Lucifer yellow).

The method used for *in vitro* transport studies and calculation of transport ratios was previously reported.[74] Shortly before the experiment, the culture medium was removed from the apical and basolateral compartments of the 96-insert plate and replaced with medium without phenol red. The measurement of transcellular transport was initiated by adding culture medium

containing 1 μM test compound to either side (100 μL on the apical side or 240 μL on the basolateral side). The transport experiment was performed in both apical-to-basolateral and basolateral-to-apical directions in triplicates on a robotic pipetting device.

The inserts were incubated at 37 °C and 5% CO_2 and 20 μL samples were taken from both the donor and receiver sides after 3.5 h of incubation. Test compound concentrations were measured by high performance liquid chromatography–tandem mass spectrometry (LC–MS/MS). The Lucifer yellow was quantified using a Spectrafluor Plus Reader at 430/535 nm excitation/emission in each insert as a control of cell tightness. Data from inserts exhibiting marker permeation >1%/h were rejected.

ASSOCIATED CONTENT

Supporting Information. Additional figures and schemes on predicted protein-ligand interactions by modeling; Polar surface area calculations; Enzymatic and parasitic results; Mouse PK curves; Antiparasitic activity against a parasite panel; *In vivo* results; Synthesis; Synthetic procedures; NMR spectra of all final compounds; Molecular formula strings. This material is available free of charge via the Internet at http://pubs.acs.org.

AUTHOR INFORMATION

Corresponding Author

* WH: Phone +41 61 68 88693. E-mail: wolfgang.haap@roche.com.

Author Contributions

The manuscript was written through contributions of all authors. All authors have given approval to the final version of the manuscript.

Funding Sources

Work was supported by F. Hoffmann-La Roche Ltd., by an F. Hoffmann-La Roche – ETH Zurich research agreement, and by the Collaborative Research Center 630 (German Research Society, DFG).

ACKNOWLEDGMENT

The authors acknowledge Markus Buerkler and Dr. Inken Plitzko from the Roche Analytics Service for measuring all NMR data, and Daniel Zimmerli for measuring the optical rotation. Björn Wagner and Virginie Micallef are acknowledged for physicochemical characterization of

the compounds. *In vitro* transport studies were conducted by Marie-Elise Brun and Dr. Silke Simon, and pharmacokinetic studies were conducted by Thomas Thelly, Marie-Stella Gruyer, Christelle Rapp, Véronique Dall'Asen and Christophe Flament. We thank Nicole Denk, Sabine Maehrlein, and Ulrike Nowe at the Johannes-Gutenberg Universität Mainz for support with the enzymatic assays, as well as Christiane Braghiroli, Monica Cal and Sonja Keller for help with the parasitic assays. Dr. Bruno Bernet is greatly acknowledged for correcting the Experimental Section.

ABBREVIATIONS

Boc, *tert*-Butoxycarbonyl; dba, (1*E*,4*E*)-1,5-diphenylpenta-1,4-dien-3-one; DMA, *N,N*-dimethylacetamide; DMF, *N,N*-dimethylformamide; EDTA = ethylenediaminetretraacetic acid; HATU, 1-[bis(dimethylamino)methylene]-1*H*-1,2,3-triazolo[4,5-b]pyridinium 3-oxide hexafluorophosphate; HMBC, heteronuclear multiple-bond correlation spectroscopy; HPLC, high pressure liquid chromatography; FC, flash chromatography; IC_{50}, half maximal inhibitory concentration; K_i, binding affinity of the inhibitor; MPLC, medium pressure liquid chromatography; NOESY, nuclear Overhauser effect spectroscopy; TFA, trifluoroacetic acid; THF, tetrahydrofuran; XPhos, 2-dicyclohexylphosphino-2′,4′,6′-triisopropylbiphenyl.

PDB ID Codes: Authors will release the atomic coordinates and experimental data upon article publication.

PDB ID	Compound Number
6EX8	**3**
6EXO	**No number assigned in this manuscript**
6EXQ	**No number assigned in this manuscript**

ORCID

François Diederich 0000-0003-1947-6327

Rainer E. Martin: 0000-0001-7895-497X

REFERENCES

(1) Brun, R.; Blum, J.; Chappuis, F.; Burri, C. Human African Trypanosomiasis. *Lancet* **2010**, *375*, 148-159.

(2) Lejon, V.; Bentivoglio, M.; Franco, J. R. Chapter 11 - Human African Trypanosomiasis. In *Handbook of Clinical Neurology*, Chapt. 11, Garcia, H. H., Tanowitz, H. B., Del Brutto, O. H., Eds.; Elsevier B. V.: 2013; Vol. 114, pp 169-181.

(3) Malvy, D.; Chappuis, F. Sleeping Sickness. *Clin. Microbiol. Infect.* **2011**, *17*, 986-995.

(4) Priotto, G.; Kasparian, S.; Mutombo, W.; Ngouama, D.; Ghorashian, S.; Arnold, U.; Ghabri, S.; Baudin, E.; Buard, V.; Kazadi-Kyanza, S.; Ilunga, M.; Mutangala, W.; Pohlig, G.; Schmid, C.; Karunakara, U.; Torreele, E.; Kande, V. Nifurtimox-Eflornithine Combination Therapy for Second-stage African *Trypanosoma brucei gambiense* Trypanosomiasis: A Multicentre, Randomised, Phase III, Non-inferiority Trial. *Lancet* **2009**, *374*, 56-64.

(5) *Target Product Profile–Sleeping Sickness;* Drugs for Neglected Diseases Initiative. http//dndi.org/disease-projects/hat/hat-target-product-profile/ (accessed January 15, 2017).

(6) Kaiser, M.; Bray, M. A.; Cal, M.; Bourdin Trunz, B.; Torreele, E.; Brun, R. Antitrypanosomal Activity of Fexinidazole, a New Oral Nitroimidazole Drug Candidate for Treatment of Sleeping Sickness. *Antimicrob. Agents Chemother.* **2011**, *55*, 5602-5608.

(7) Jones, D. C.; Foth, B. J.; Urbaniak, M. D.; Patterson, S.; Ong, H. B.; Berriman, M.; Fairlamb, A. H. Genomic and Proteomic Studies on The Mode of Action of Oxaboroles Against The African Trypanosome. *PLoS Negl. Trop. Dis.* **2015**, *9*(12), e0004299.

(8) Burri, C.; Yeramian, P. D.; Allen, J. L.; Merolle, A.; Serge, K. K.; Mpanya, A.; Lutumba, P.; Mesu, V. K. B. K.; Bilenge, C. M. M.; Lubaki, J.–P. F.; Mpoto, A. M.; Thompson, M.; Mununguu, B.F.; Manuel, F.; Josenando, T.; Bernhard, S. C.; Olson, C. A.; Blum, J.; Tidwell, R. R.; Pohlig, G. Efficacy, Safety, and Dose of Pafuramidine, a New Oral Drug for Treatment of First Stage Sleeping Sickness, in a Phase 2a Clinical Study and Phase 2b Randomized Clinical Studies. *PLoS Negl. Trop. Dis.* **2016** *10* (2), e0004362.

(9) Pohlig, G.; Bernhard, S. C.; Blum, J.; Burri, C.; Mpanya, A.; Lubaki, J.–P.; Mpoto, A. M.; Mununguu, B. F.; N'tombe, P. M.; Deo, G. K.; Mutantu, P. N.; Kuikumbi, F. M.; Mintwo, A. F.; Mununguu, A. K.; Dala, A.; Macharia, S.; Bilenge, C. M.; Mesu, V. K.; Franco, J. R.; Dituvanga, N. D.; Tidwell, R. R.; Olson, C. A. Efficacy and Safety of Pafuramidine versus Pentamidine Maleate for Treatment of First Stage Sleeping Sickness in a Randomized, Comparator-Controlled, International Phase 3 Clinical Trial. *PLoS Negl. Trop. Dis*. **2016** *10*(2), e0004363.

(10) Volkov, O. A.; Brockway, A. J.; Wring, S. A.; Peel, M.; Chen, Z.; Phillips, M. A.; De Brabander, J. K. Species-Selective Pyrimidineamine Inhibitors of *Trypanosoma brucei* S-Adenosylmethionine Decarboxylase. *J. Med. Chem.* **2018**, *61*, 1182-1203.

(11) Fueyo González, F. G.; Ebiloma, G. U.; Izquierdo García, C.; Bruggeman, V.; Sánchez Villamañán, J. M.; Donachie, A.; Oluwadare Balogun, E.; Inaoka, D. K.; Shiba, T.; Harada, S.; Kita, K.; de Koning, H. P.; Dardonville, C. Conjugates of 2,4-

Dihydroxybenzoate and Salicylhydroxamate and Lipocations Display Potent Antiparasite Effects by Efficiently Targeting the *Trypanosoma brucei* and *Trypanosoma congolense* Mitochondrion. *J. Med. Chem.* **2017**, *60*, 1509-1522.

(12) Patrick, D. A.; Gillespie, J. R.; McQueen, J.; Hulverson, M. A.; Ranade, R. M.; Creason, S. A.; Herbst, Z. M.; Gelb, M. H.; Buckner, F. S.; Tidwell, R. R. Urea Derivatives of 2-Aryl-benzothiazol-5-amines: A New Class of Potential Drugs for Human African Trypanosomiasis. *J. Med. Chem.* **2017**, *60*, 957-971.

(13) Russell, S.; Rahmani, R.; Jones, A. J.; Newson, H. L.; Neilde, K.; Cotillo, I.; Rahmani Khajouei, M.; Ferrins, L.; Qureishi, S.; Nguyen, N.; Martinez-Martinez, M. S.; Weaver, D. F.; Kaiser, M.; Riley, J.; Thomas, J.; De Rycker, M.; Read, K. D.; Flematti, G. R.; Ryan, E.; Tanghe, S.; Rodriguez, A.; Charman, S. A.; Kessler, A.; Avery, V. M.; Baell, J. B.; Piggott, M. J. Hit-to-Lead Optimization of a Novel Class of Potent, Broad-Spectrum Trypanosomacides. *J. Med. Chem.* **2016**, *59*, 9686-9720.

(14) Cleghorn, L. A. T.; Albrecht, S.; Stojanovski, L.; Simeons, F. R. J.; Norval, S.; Kime, R.; Collie, I. T.; De Rycker, M.; Campbell, L.; Hallyburton, I.; Frearson, J. A.; Wyatt, P. G.; Read, K. D.; Gilbert, I. H. Discovery of Indoline-2-carboxamide Derivatives as a New Class of Brain-Penetrant Inhibitors of *Trypanosoma brucei*. *J. Med. Chem.* **2015**, *58*, 7695-7706.

(15) Nicoll-Griffith, D. A. Use of Cysteine-reactive Small Molecules in Drug Discovery for Trypanosomal Disease. *Expert Opin. Drug Disc.* **2012**, *7*, 353-366.

(16) Kerr, I. D.; Lee, J. H.; Farady, C. J.; Marion, R.; Rickert, M.; Sajid, M.; Pandey, K. C.; Caffrey, C. R.; Legac, J.; Hansell, E.; McKerrow, J. H.; Craik, C. S.; Rosenthal, P. J.;

Brinen, L. S. Vinyl Sulfones as Antiparasitic Agents and a Structural Basis for Drug Design. *J. Biol. Chem.* **2009**, *284*, 25697-25703.

(17) Kerr, I. D.; Wu, P.; Marion-Tsukamaki, R.; Mackey, Z. B.; Brinen, L. S. Crystal Structures of TbCatB and Rhodesain, Potential Chemotherapeutic Targets and Major Cysteine Proteases of *Trypanosoma brucei*. *PLoS Negl. Trop. Dis.* **2010**, *4*(6), e701.

(18) Reyes-López, M.; Piña-Vázquez C.; Serrano-Luna J. Transferrin: Endocytosis and Cell Signaling in Parasitic Protozoa. *BioMed Research International*, **2015**, Article ID 641392.

(19) Ettari, R.; Previti, S.; Tamborini, L.; Cullia, G.; Grasso, S.; Zappala, M. The Inhibition of Cysteine Proteases Rhodesain and TbCatB: A Valuable Approach to Treat Human African Trypanosomiasis. *Mini-Rev. Med. Chem.* **2016**, *16*, 1374-1391.

(20) Ettari, R.; Tamborini, L.; Angelo, I. C.; Micale, N.; Pinto, A.; De Micheli, C.; Conti, P. Inhibition of Rhodesain as a Novel Therapeutic Modality for Human African Trypanosomiasis. *J. Med. Chem.* **2013**, *56*, 5637-5658.

(21) Greenspan, P. D.; Clark, K. L.; Cowen, S. D.; McQuire, L. W.; Tommasi, R. A.; Farley, D. L.; Quadros, E.; Coppa, D. E.; Du, Z.; Fang, Z.; Zhou, H.; Doughty, J.; Toscano, K. T.; Wigg, A. M.; Zhou, S. *N*-Arylaminonitriles as Bioavailable Peptidomimetic Inhibitors of Cathepsin B. *Bioorg. Med. Chem. Lett.* **2003**, *13*, 4121-4124.

(22) Greenspan, P. D.; Clark, K. L.; Tommasi, R. A.; Cowen, S. D.; McQuire, L. W.; Farley, D. L.; van Duzer, J. H.; Goldberg, R. L.; Zhou, H.; Du, Z.; Fitt, J. J.; Coppa, D. E.; Fang, Z.; Macchia, W.; Zhu, L.; Capparelli, M. P.; Goldstein, R.; Wigg, A. M.; Doughty, J. R.;

Bohacek, R. S.; Knap, A. K. Identification of Dipeptidyl Nitriles as Potent and Selective Inhibitors of Cathepsin B through Structure-Based Drug Design. *J. Med. Chem.* **2001**, *44*, 4524-4534.

(23) Guay, D.; Beaulieu, C.; Reddy, T. J.; Zamboni, R.; Methot, N.; Rubin, J.; Ethier, D.; Percival, M. D. Design and Synthesis of Dipeptidyl Nitriles as Potent, Selective, and Reversible Inhibitors of Cathepsin C. *Bioorg. Med. Chem. Lett.* **2009**, *19*, 5392-5396.

(24) Altmann, E.; Aichholz, R.; Betschart, C.; Buhl, T.; Green, J.; Lattmann, R.; Missbach, M. Dipeptide Nitrile Inhibitors of Cathepsin K. *Bioorg. Med. Chem. Lett.* **2006**, *16*, 2549-2554.

(25) Asaad, N.; Bethel, P. A.; Coulson, M. D.; Dawson, J. E.; Ford, S. J.; Gerhardt, S.; Grist, M.; Hamlin, G. A.; James, M. J.; Jones, E. V.; Karoutchi, G. I.; Kenny, P. W.; Morley, A. D.; Oldham, K.; Rankine, N.; Ryan, D.; Wells, S. L.; Wood, L.; Augustin, M.; Krapp, S.; Simader, H.; Steinbacher, S. Dipeptidyl Nitrile Inhibitors of Cathepsin L. *Bioorg. Med. Chem. Lett.* **2009**, *19*, 4280-4283.

(26) Gauthier, J. Y.; Black, W. C.; Courchesne, I.; Cromlish, W.; Desmarais, S.; Houle, R.; Lamontagne, S.; Li, C. S.; Massé, F.; McKay, D. J.; Ouellet, M.; Robichaud, J.; Truchon, J.-F.; Truong, V.-L.; Wang, Q.; Percival, M. D. The Identification of Potent, Selective, and Bioavailable Cathepsin S Inhibitors. *Bioorg. Med. Chem. Lett.* **2007**, *17*, 4929-4933.

(27) Avelar, L. A. A.; Camilo, C. D.; de Albuquerque, S.; Fernandes, W. B.; Gonçalez, C.; Kenny, P. W.; Leitão, A.; McKerrow, J. H.; Montanari, C. A.; Meñaca Orozco, E. V.; Ribeiro, J. F. R.; Rocha, J. R.; Rosini, F.; Saidel, M. E. Molecular Design, Synthesis and

Trypanocidal Activity of Dipeptidyl Nitriles as Cruzain Inhibitors. *PLoS Negl. Trop. Dis.* **2015**, *9* (7), e0003916.

(28) Ehmke, V.; Kilchmann, F.; Heindl, C.; Cui, K.; Huang, J.; Schirmeister, T.; Diederich, F. Peptidomimetic Nitriles as Selective Inhibitors for the Malarial Cysteine Protease Falcipain-2. *Med. Chem. Commun.* **2011**, *2*, 800-804.

(29) Schirmeister, T.; Schmitz, J.; Jung, S.; Schmenger, T.; Krauth-Siegel, R. L.; Gütschow, M. Evaluation of Dipeptide Nitriles as Inhibitors of Rhodesain, A Major Cysteine Protease of *Trypanosoma brucei*. *Bioorg. Med. Chem. Lett.* **2017**, *27*, 45-50.

(30) Dufour, E.; Storer, A. C.; Ménard, R. Peptide Aldehydes and Nitriles as Transition State Analog Inhibitors of Cysteine Proteases. *Biochemistry* **1995**, *34*, 9136-9143.

(31) Giroud, M.; Dietzel, U.; Anselm, L.; Banner, D.; Kuglstatter, A.; Benz, J.; Blanc, J.-B.; Gaufreteau, D.; Liu, H.; Lin, X.; Stich, A.; Kuhn, B.; Schuler, F.; Kaiser, M.; Brun, R.; Schirmeister, T.; Kisker, C.; Diederich, F.; Haap, W. Repurposing a Library of Human Cathepsin L Ligands: Identification of Macrocyclic Lactams as Potent Rhodesain and *Trypanosoma brucei* Inhibitors, *unpublished results*.

(32) Schinkel, A. H. P-Glycoprotein, A Gatekeeper in the Blood-Brain-Barrier. *Adv. Drug. Deliv. Rev.* **1999**, *36*, 179-194.

(33) Gerber, P. R.; Müller, K. MAB, A Generally Applicable Molecular Force Field For Structure Modelling In Medicinal Chemistry. *J. Comput.-Aided Mol. Des.* **1995**, *9*, 251-268.

(34) Hardegger, L. A.; Kuhn, B.; Spinnler, B.; Anselm, L.; Ecabert, R.; Stihle, M.; Gsell, B.; Thoma, R.; Diez, J.; Benz, J.; Plancher, J.-M.; Hartmann, G.; Banner, D. W.; Haap, W.; Diederich, F. Systematic Investigation of Halogen Bonding in Protein-Ligand Interactions. *Angew. Chem., Int. Ed.* **2011**, *50*, 314-318.

(35) Ehmke, V.; Heindl, C.; Rottmann, M.; Freymond, C.; Schweizer, W. B.; Brun, R.; Stich, A.; Schirmeister, T.; Diederich, F. Potent and Selective Inhibition of Cysteine Proteases from *Plasmodium falciparum* and *Trypanosoma brucei*. *ChemMedChem* **2011**, *6*, 273-278.

(36) Giordanetto, F.; Tyrchan, C.; Ulander, J. Intramolecular Hydrogen Bond Expectations in Medicinal Chemistry. *ACS Med. Chem. Lett.* **2017**, *8*, 139-142.

(37) Kuhn, B.; Mohr, P.; Stahl, M. Intramolecular Hydrogen Bonding in Medicinal Chemistry. *J. Med. Chem.* **2010**, *53*, 2601-2611.

(38) Baldwin, I. R.; Down, K. R.; Faulder, P.; Gaines, S.; Hamblin, J. N.; Le, J.; Lunniss, C. J.; Parr, N. J.; Ritchie, T. J.; Robinson, J. E.; Simpson, J. K.; Smethurst, C. A. P. Benzylpyrazol Derivatives as Inhibitors of PI3 Kinases. WO 2009/147188 A1, 2009.

(39) Anisimova, N. A.; Berestovitskaya, V. M.; Berkova, G. A.; Makarova, N. G. Reaction of 3-Nitro-and 3-Bromo-3-nitroacrylates With Sodium Azide. *Russ. J. Org. Chem.* **2007**, *43*, 652-655.

(40) Galley, G.; Ghellamallah, C.; Norcross, R.; Pflieger, P. Triazole Carboxamide Derivatives. WO2014041106 A1, 2014.

(41) Taherpour, A. A.; Kheradmand, K. One-pot Microwave-assisted Solvent Free Synthesis of Simple Alkyl 1,2,3-Triazole-4-carboxylates by Using Trimethylsilyl Azide. *J. Het. Chem.* **2009**, *46*, 131-133.

(42) Bräse, S.; Gil, C.; Knepper, K.; Zimmermann, V. Organic Azides: An Exploding Diversity of a Unique Class of Compounds. *Angew. Chem., Int. Ed.* **2005**, *44*, 5188-5240.

(43) Ötvös, S. B.; Fülöp, F. Flow Chemistry as a Versatile Tool for the Synthesis of Triazoles. *Catal. Sci. Technol.* **2015**, *5*, 4926-4941.

(44) Baumann, M.; Baxendale, I. R. The Synthesis of Active Pharmaceutical Ingredients (APIs) Using Continuous Flow Chemistry. *Beilstein J. Org. Chem.* **2015**, *11*, 1194-1219.

(45) Belskaya, N.; Subbotina, J.; Lesogorova, S. Synthesis of 2*H*-1,2,3-Triazoles. In *Topics in Heterocyclic Chemistry*; Dehaen, W., Bakulev, V. A., Eds.; Springer-Verlag: Berlin, 2015; Vol 40, pp 51-116.

(46) Ueda, S.; Su, M.; Buchwald, S. L. Highly N^2-Selective Palladium-Catalyzed Arylation of 1,2,3-Triazoles. *Angew. Chem., Int. Ed.* **2011**, *50*, 8944-8947.

(47) Chan, D. M. T.; Monaco, K. L.; Wang, R.-P.; Winters, M. P. New N- and O-Arylations With Phenylboronic Acids and Cupric Acetate. *Tetrahedron Lett.* **1998**, *39*, 2933-2936.

(48) Evans, D. A.; Katz, J. L.; West, T. R. Synthesis of Diaryl Ethers Through the Copper-promoted Arylation of Phenols With Arylboronic Acids. An Expedient Synthesis of Thyroxine. *Tetrahedron Lett.* **1998**, *39*, 2937-2940.

(49) Lam, P. Y. S.; Clark, C. G.; Saubern, S.; Adams, J.; Winters, M. P.; Chan, D. M. T.; Combs, A. New Aryl/Heteroaryl C-N Bond Cross-coupling Reactions *via* Arylboronic Acid/Cupric Acetate Arylation. *Tetrahedron Lett.* **1998**, *39*, 2941-2944.

(50) Kalisiak, J.; Sharpless, K. B.; Fokin, V. V. Efficient Synthesis of 2-Substituted-1,2,3-triazoles. *Org. Lett.* **2008**, *10*, 3171-3174.

(51) Regitz, M.; Schoder, W. Untersuchungen an Diazo-Verbindungen und Aziden; LVI. Amino- und Iminomethylierung von Diazomethyl-Verbindungen. *Synthesis* **1985**, *1985*, 178-180.

(52) El Khadem, H.; Meshreki, M. H.; Labib, G. H. The Scope and Mechanism of Carbohydrate Osotriazole Formation. Part XII. Anhydro- and Other Triazole Derivatives. *J. Chem. Soc.* **1964**, 2306-2309.

(53) Danoun, S.; Baziard-Mouysset, G.; Stigliani, J.-L.; Commenges, G.; Carpy, A.; Payard, M. Study of the Reactivity of Nitriles Towards Diazomethane: Synthesis and Structural Study of *N*-Methyl-v-Triazoles. *Bull. Soc. Chim. France* **1995**, *132*, 943-951.

(54) L'abbé, G.; Bruynseels, M.; Delbeke, P.; Toppet, S. Molecular Rearrangements of 4-Iminomethyl-1,2,3-triazoles. Replacement of 1-Aryl Substituents in 1*H*-1,2,3-Triazole-4-Carbaldehydes. *J. Heterocyclic Chem.* **1990**, *27*, 2021-2027.

(55) Ali, A. A.; Chetia, M.; Saikia, B.; Saikia, P. J.; Sarma, D. $AgN(CN)_2$/DIPEA/H_2O-EG: A Highly Efficient Catalytic System for Synthesis of 1,4-Disubstituted-1,2,3 Triazoles at Room Temperature. *Tetrahedron Lett.* **2015**, *56*, 5892-5895.

(56) Giroud, M.; Harder, M.; Kuhn, B.; Haap, W.; Trapp, N.; Schweizer, W. B.; Schirmeister, T.; Diederich, F. Fluorine Scan of Inhibitors of the Cysteine Protease Human Cathepsin L: Dipolar and Quadrupolar Effects in the π-Stacking of Fluorinated Phenyl Rings on Peptide Amide Bonds. *ChemMedChem* **2016**, *11*, 1042-1047.

(57) Giroud, M.; Ivkovic, J.; Martignoni, M.; Fleuti, M.; Trapp, N.; Haap, W.; Kuglstatter, A.; Benz, J.; Kuhn, B.; Schirmeister, T.; Diederich, F. Inhibition of the Cysteine Protease Human Cathepsin L by Triazine Nitriles: Amide□□□Heteroarene π-Stacking Interactions and Chalcogen Bonding in the S3 Pocket. *ChemMedChem* **2017**, *12*, 257-270.

(58) Ludewig, S.; Kossner, M.; Schiller, M.; Baumann, K.; Schirmeister, T. Enzyme Kinetics and Hit Validation in Fluorimetric Protease Assays. *Curr. Top. Med. Chem.* **2010**, *10*, 368-382.

(59) Räz, B.; Iten, M.; Grether-Bühler, Y.; Kaminsky, R.; Brun, R. The Alamar Blue® Assay to Determine Drug Sensitivity of African Trypanosomes (*T.b. rhodesiense* and *T.b. gambiense*) In Vitro. *Acta Tropica* **1997**, *68*, 139-147.

(60) Wagner, B.; Fischer, H.; Kansy, M.; Seelig, A.; Assmus, F. Carrier Mediated Distribution System (CAMDIS): A New Approach for the Measurement of Octanol/Water Distribution Coefficients. *Eur. J. Pharm. Sci.* **2015**, *68*, 68-77.

(61) Wuitschik, G.; Carreira, E. M.; Wagner, B.; Fischer, H.; Parrilla, I.; Schuler, F.; Rogers-Evans, M.; Müller, K. Oxetanes in Drug Discovery: Structural and Synthetic Insights. *J. Med. Chem.* **2010**, *53*, 3227-3246.

(62) Orhan, I.; Şener, B.; Kaiser, M.; Brun, R.; Tasdemir, D. Inhibitory Activity of Marine Sponge-Derived Natural Products against Parasitic Protozoa. *Mar. Drugs* **2010**, *8*(1), 47-58.

(63) Brun, R.; Don, R.; Jacobs, R. T.; Wang, M. Z.; Barrett, M. P. Development of Novel Drugs for Human African Trypanosomiasis. *Future Microbiol.* **2011**, *6*, 677-691.

(64) Ertl, P.; Rohde, B.; Selzer, P. Fast Calculation of Molecular Polar Surface Area As A Sum of Fragment Based Contributions And Its Application To The Prediction of Drug Transport Properties, *J. Med. Chem.* **2000**, *43*, 3714-3717.

(65) Wager, T. T.; Hou, X.; Verhoest, P. R.; Villalobos, A. Moving Beyond Rules: The Development of a Central Nervous System Multiparameter Optimization (CNS MPO) Approach To Enable Alignment of Druglike Properties. *ACS Chem. Neurosci.* **2010**, *1*, 435-449.

(66) Brooks, D. R.; Tetley, L.; Coombs, G. H.; Mottram, J. C. Processing and Trafficking of Cysteine Proteases in *Leishmania mexicana, J. Cell. Sci.* **2000**, *113*, 4035-4041.

(67) Ndao, M.; Beaulieu, C.; Black, W. C.; Isabel, E.; Vasquez-Camargo, F.; Nath-Chowdhury, M.; Massé, F.; Mellon, C.; Methot, N.; Nicoll-Griffith, D. A. Reversible Cysteine Protease Inhibitors Show Promise for a Chagas Disease Cure. *Antimicrob. Agents Chemother.* **2014**, *58*, 1167-1178.

(68) Rosenthal, P. J. Falcipains and Other Cysteine Proteases of Malaria Parasites. In: Robinson, M. W.; Dalton, J. P., Eds.; Springer: Boston, MA, 2011; Vol. 712.

(69) Cheng, Y.-C.; Prusoff, W. H. Relationship Between The Inhibition Constant (K_i) and the Concentration of Inhibitor Which Causes 50 Per Cent Inhibition (IC_{50}) of an Enzymatic Reaction. *Biochem. Pharmacol.* **1973**, *22*, 3099-3108.

(70) Räz, B.; Iten, M.; Grether-Bühler, Y.; Kaminsky, R.; Brun, R. The Alamar Blue Assay to Determine Drug Sensitivity of African Trypanosomes (*T. b. rhodesiense* and *T. b. gambiense*) In Vitro. *Acta Trop.* **1997**, *68*, 139-147.

(71) Huber, W.; Koella, J. C. A Comparison of Three Methods of Estimating EC_{50} in Studies of Drug Resistance of Malaria Parasites. *Acta Trop.* **1993**, *55*, 257-261.

(72) Kansy, M.; Senner, F.; Gubernator, K. Physicochemical High Throughput Screening: Parallel Artificial Membrane Permeation Assay in the Description of Passive Absorption Processes. *J. Med. Chem.* **1998**, *41*, 1007-1010.

(73) Fowler, S.; Zhang, H. *In Vitro* Evaluation of Reversible and Irreversible Cytochrome P450 Inhibition: Current Status on Methodologies and their Utility for Predicting Drug–Drug Interactions. *AAPS J.* **2008**, *10*, 410-424.

(74) Schwab, D.; Fischer, H.; Tabatabaei, A.; Poli, S.; Huwyler, J. Comparison of in Vitro P-Glycoprotein Screening Assays: Recommendations for Their Use in Drug Discovery. *J. Med. Chem.* **2003**, *46*, 1716-1725.

TABLE OF CONTENTS GRAPHIC

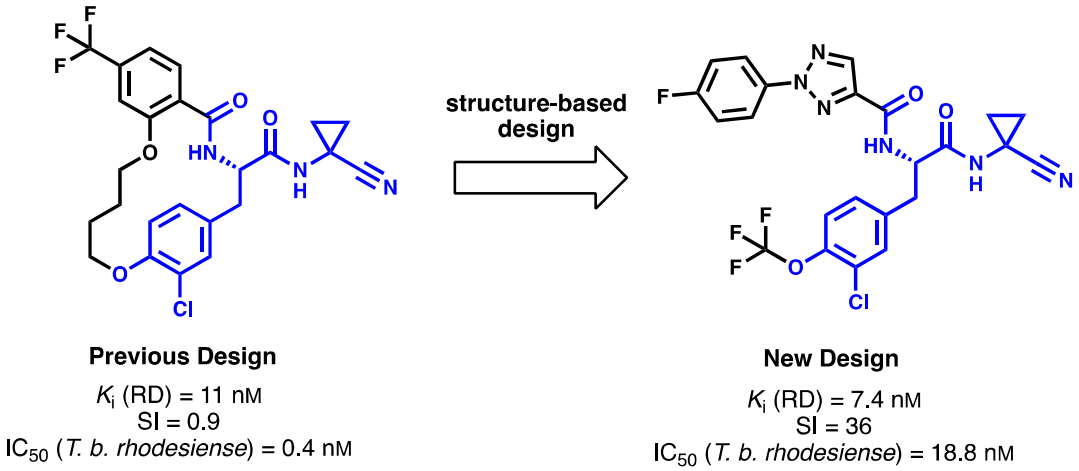

• simplified synthesis • improved selectivity (SI) against hCatL • improved P-gp ER

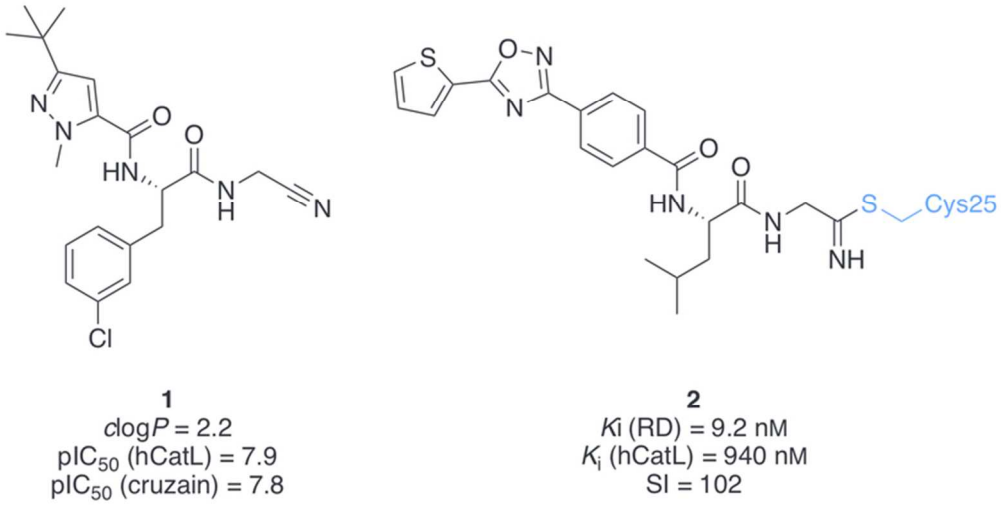

Figure 1. Known dipeptidyl nitriles inhibiting the cysteine proteases hCatL and cruzain (1), and RD (2). The thioimidate bond formed upon nucleophilic attack by Cys25 of RD is exemplified for 2.

69x34mm (300 x 300 DPI)

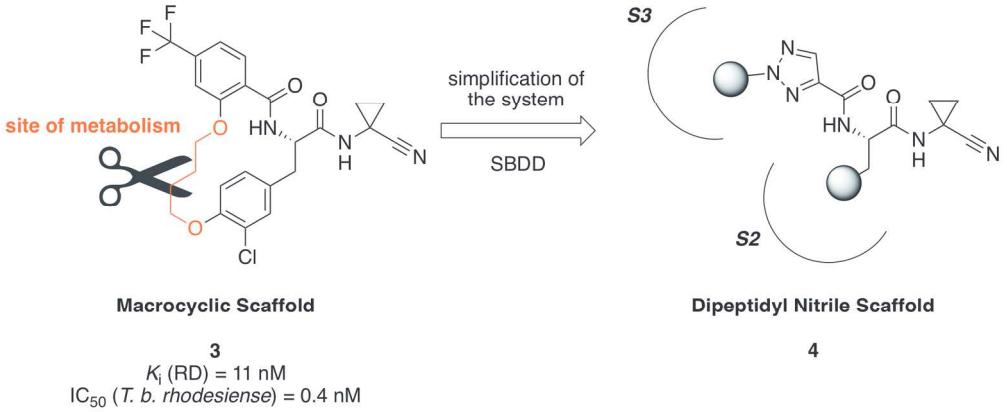

Figure 2. Simplification of the macrocyclic scaffold, as in 3, towards dipeptidyl nitriles 4.

176x72mm (300 x 300 DPI)

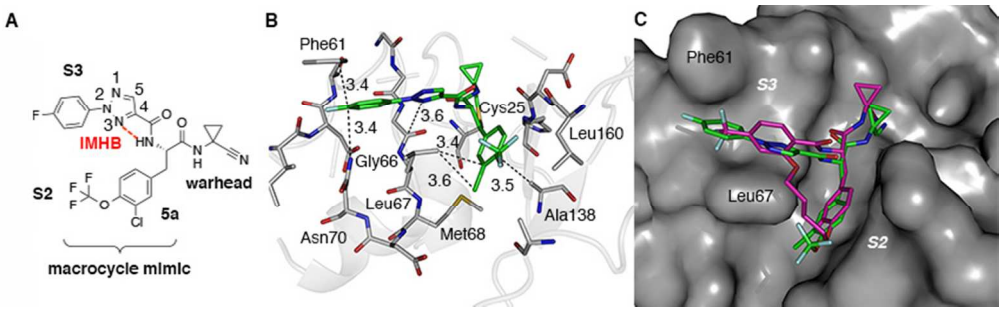

Figure 3. (A) Schematic representation of designed dipeptidyl nitrile 5a; (B) predicted binding mode of 5a in complex with RD (protein coordinates taken from PDB ID:25 6EX8, 1.6 Å resolution); (C) overlay of the crystal structure of macrocycle 3 in complex with RD (PDB ID:25 6EX8, 1.6 Å resolution) with the model of 5a. Color code: C3 magenta, C5a green, O red, N blue, F cyan. The protein surface around the active site of RD in the crystal structure is represented in gray.

299x89mm (72 x 72 DPI)

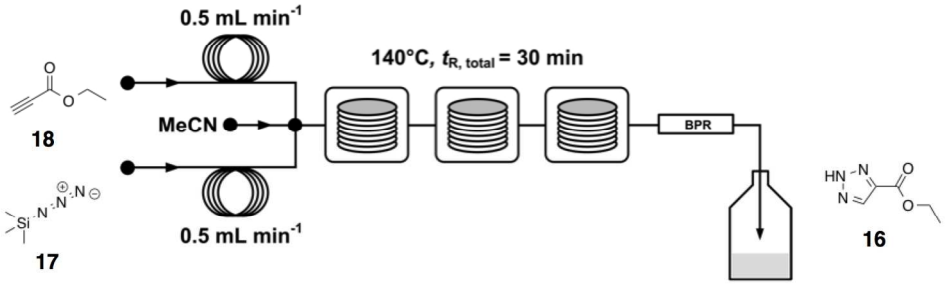

Figure 4. Plug flow process for the production of ethyl 1H-1,2,3-triazole-4-carboxylate (16).

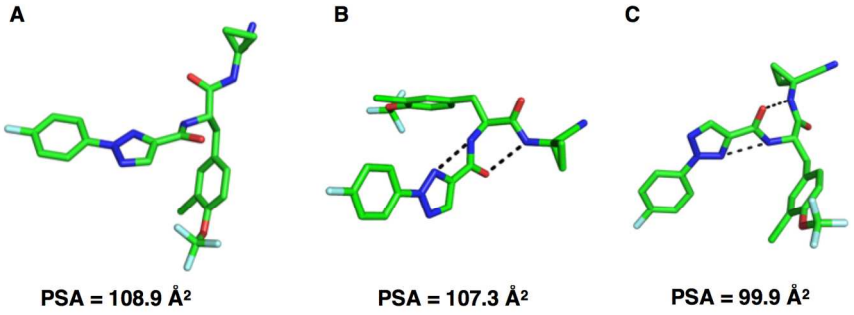

Figure 5. Conformation of dipeptidyl nitrile 5a in the (A) bound conformation (extracted from the predicted binding mode in RD, protein coordinates taken from PDB ID:3 6EX8, 1.6 Å resolution); (B) low energy conformation in the unbound state generated with Mol3d; (C) unbound conformation using a MM conformational search with subsequent QM optimization. Polar surface areas were calculated with the MOLOC companion program Msrfvl. Color code: green C5a,bound, cyan C5a,unbound, red O, blue N, lime Cl, light blue F. Distances represented by dotted black lines and given in Å.

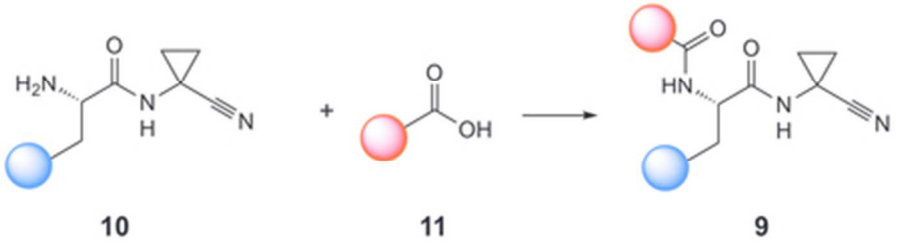

Scheme 1. General Approach for the Preparation of Dipeptides 9.a

37x10mm (300 x 300 DPI)

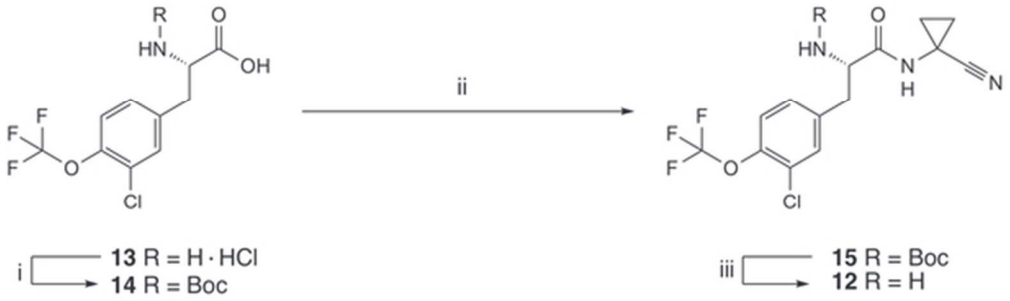

Scheme 2. Preparation of Building Block 12.a

51x15mm (300 x 300 DPI)

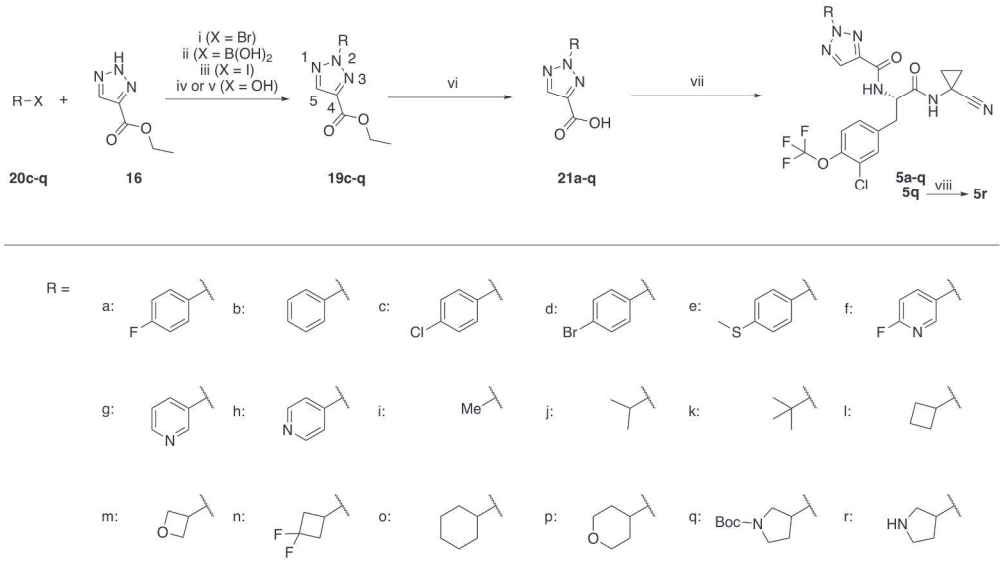

Scheme 3. Preparation of Dipeptidyl Nitriles 5a–ra

240x133mm (300 x 300 DPI)

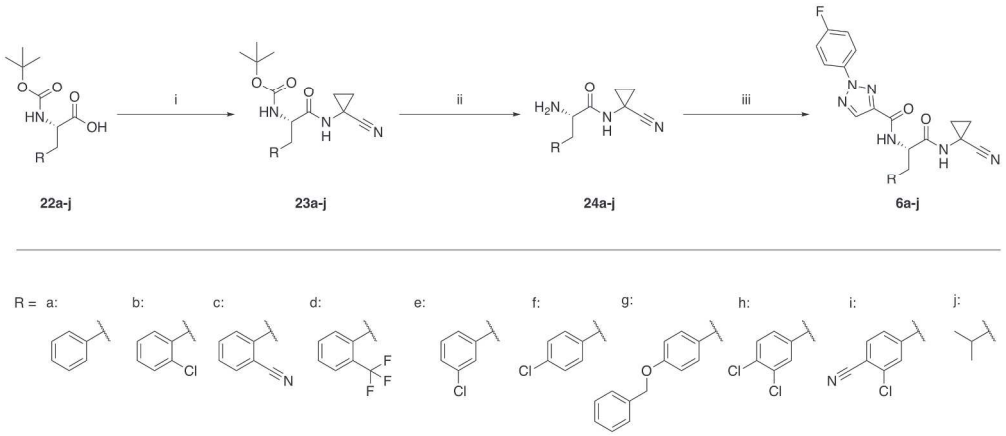

Scheme 4. Synthesis of Dipeptidyl Nitriles 6a–ja

253x109mm (300 x 300 DPI)

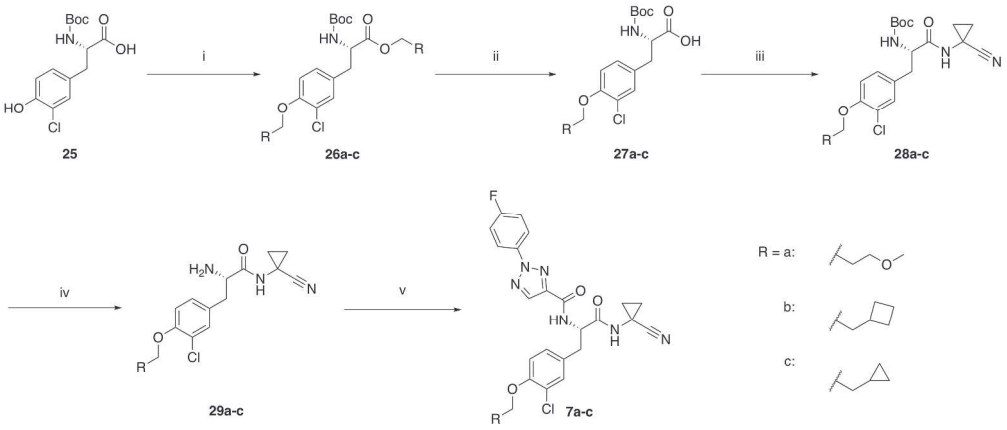

Scheme 5. Synthesis of Dipeptidyl Nitriles 7a–ca

258x109mm (300 x 300 DPI)

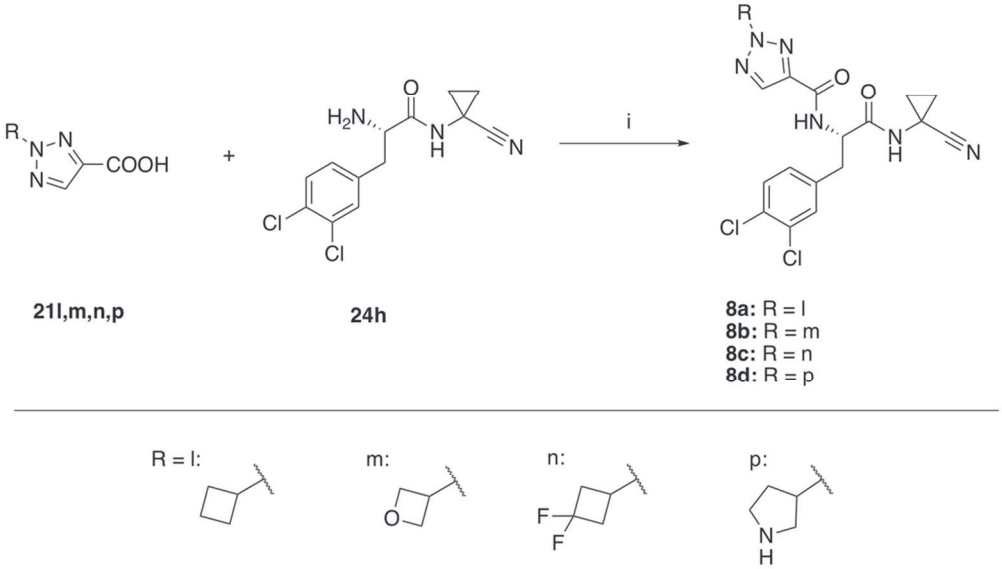

Scheme 6. Synthesis of Dipeptidyl Nitriles 8a–da

95x54mm (300 x 300 DPI)

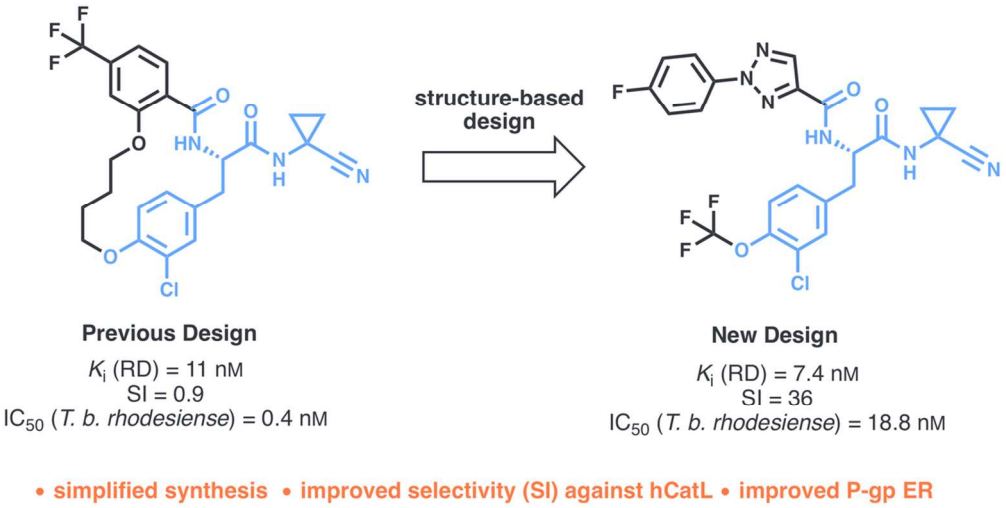

Table of Content graphic

109x54mm (300 x 300 DPI)